The Quantum Geometry of Spacetime

X. Aupí

Institut Illa de Rodes, Roses, 17480, Catalonia, Spain.

Contributing authors: xaviaupi@gmail.com;

Abstract

This article forms the second part of the study entitled *The Fundamental Cycle: A Harmonic Reinterpretation of Relativity and Its Cosmological Implications*. Whereas the first part focused on macroscopic systems, the present work applies the same universal framework at the microscopic level. We begin by emphasizing the wave-like nature of relativity. Subsequently, we provide a geometric derivation of the de Broglie and Planck-Einstein relations. This derivation leads to a representation of particles as sets of rotating elements in spacetime. Next, we derive the uncertainty principle within the relativistic framework, contingent upon the following experimentally testable conjecture: there exist specific momentum values for which a particle becomes unobservable. We then introduce discrete time, which refines the earlier conception of particles as sets of continuously rotating elements into a model of discrete rotation. In this model, the elements undergo a collective cyclic exchange along the vertices of a regular polygon—or, more generally, a regular star polygon—in synchrony with the tick of proper time. This structure provides the foundation for defining spin as an intrinsic property emerging from the cyclic symmetry of the particle's internal dynamics within discrete spacetime. Once spin is established, we derive the fundamental relation $\boldsymbol{hf_o = m_o c^2}$. Finally, a quantum-level expression for gravity is obtained.

Keywords: Discrete spacetime, spin, quantum gravity

1 Introduction

The tension between relativity and quantum mechanics remains one of the central challenges of modern theoretical physics. While the former describes the continuous geometry of spacetime at macroscopic scales, the latter reveals a discrete and probabilistic nature of matter and energy at microscopic scales. Bridging these two regimes has motivated numerous theoretical frameworks, from string theory [1–4] and loop quantum gravity [5–16] to more recent attempts involving spacetime discreteness and information-theoretic principles [17].

In a preceding work [18], we introduced the concept of the *fundamental cycle* as a harmonic reinterpretation of relativity, highlighting its macroscopic implications through a global vibrational scheme. The present article extends that same conceptual structure to the microscopic level. The goal is to explore how the notion of discrete spacetime rotations might naturally give

rise to quantum mechanical features such as the uncertainty principle, wave-particle duality, spin, and even gravity.

This particular line of inquiry begins in 1908, when Minkowski [19] introduced a formalism for special relativity in terms of a rotation by an imaginary angle:

$$x' = x\cos i\theta + ict\sin i\theta \tag{1}$$

$$ict' = -x\sin i\theta + ict\cos i\theta \tag{2}$$

The presence of the imaginary unit in this expression was interpreted previously in Ref. [18]. It was suggested that it is a consequence of the fact that we, as observers, are inherently part of the observed reality. This embeddedness in the structure implies a natural split of reality into two domains or poles of duality: one that is observable and physically manifest as space, and another that lies beyond our direct observational reach and appears to us as time. The latter, inaccessible from within the structure, was algebraically represented by the imaginary unit to account for its inherent inconceivability. The imaginary unit i in Minkowski's formulation was thus proposed to reflect, at an algebraic level, the dual structure of reality—one that distinguishes between the observable domain of space and an unobservable, imaginary domain corresponding to time.

Moreover, the circular structure of Minkowski's transformation was attributed to the dynamic interplay between these two poles of duality: a continuous cycle of mutual conversion, physically manifesting as a spacetime rotation. This universal dynamical process was referred to as the *fundamental cycle*, as it was hypothesized to occur across all scales. In particular, its projection onto the real (spatial) axis turned out to give rise to a complex-valued simple harmonic motion (SHM*), from which both relativistic dynamics and gravitational phenomena can be derived. In this way, what we termed the *harmonic reinterpretation of relativity* was introduced.

When this framework was applied to the largest conceivable scale, it led to a cosmological model in which the largest structures in the Universe—such as galaxy clusters—rotate in a global spacetime with the same angular frequency and radius of curvature, though exhibiting relative phase shifts. The perspective of one of these massive bodies with respect to the rest of the structure gave rise to the cosmological picture itself.

In the present article, we extend this same universal model to the microscopic scale. Specifically, we show that a fundamental particle can be interpreted as a kind of many-body or collective motion [20–27], where a set of n elements perform a rotation in spacetime. In this microscopic context, the rotation turns out to be discrete and is characterized by a so-called *step size* m. These two quantities, n and m, will be shown to correspond to the quantum numbers associated with angular momentum.

From this new representation, we derive the fundamental relation $hf_o = m_o c^2$ [20, 28–32], linking mass, frequency, energy and spin. Finally, by incorporating this result into a relativistic generalization of centripetal acceleration, we arrive at a quantum expression for gravitational acceleration. This formulation preserves the structure $g = c^2/R$ even in the microscopic domain, suggesting a harmonic route to quantum gravity that is both conceptually and mathematically efficient.

The implications of this framework could extend beyond particle physics, potentially offering new insights into the early universe, where quantum behaviour and extreme spacetime curvature are intimately connected [33–35].

2 Wave-Like Features of Special Relativity

Typically, the wave-like character of special relativity is revealed by combining the energy-momentum relation with the de Broglie and Planck-Einstein relations, yielding both group and

phase velocities [28]:

$$\frac{d\omega}{dk} = \frac{dE}{dp} = \frac{d}{dp}\sqrt{(m_o c^2)^2 + (cp)^2} = \frac{c^2 p}{E} = \frac{c^2 m_o v_g \gamma}{m_o c^2 \gamma} = v_g$$
$$\frac{\omega}{k} = \frac{E}{p} = \frac{m_o c^2 \gamma}{m_o v_g \gamma} = \frac{c^2}{v_g} = v_p$$

From the first expression, we observe that the group velocity corresponds to the actual velocity of the particle, which is consistent with quantum mechanics. On the other hand, the second expression implies that $E = \hbar\omega_p$ and $p = \hbar k_p$, indicating that the particle's energy and momentum are intrinsically linked to the phase wave.

At first glance, one might assume that it is quantum relations that impose a wave-like structure on relativistic dynamics. However, we will now demonstrate that this wave-like behavior is an inherent feature of relativity itself. To this end, it is convenient to consider two specific values of the angle θ in the Minkowski rotation (1)–(2):

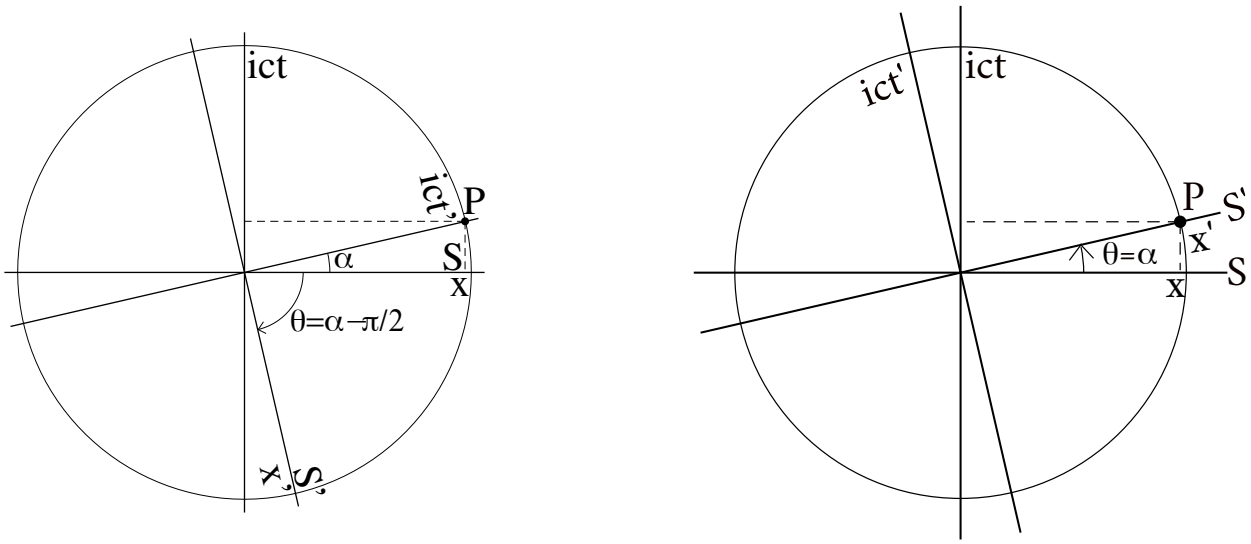

Fig. 1 **Left**: The S'-axes rotate clockwise by $\pi/2 - \alpha$, aligning the time axis with point P, so $\theta = -(\pi/2 - \alpha)$. **Right**: The S'-axes rotate counterclockwise by α, aligning the spatial axis with point P, so $\theta = \alpha$.

- When the time axis is aligned with point P, as shown in Fig. 1-*Left*, we have $x' = 0$ and $\theta = \alpha - \pi/2$. Substituting into equation (1) gives a quantity with units of velocity:[1]

$$\frac{x}{t} = -ic\frac{\sin i(\alpha - \pi/2)}{\cos i(\alpha - \pi/2)} = ic\frac{\cos i\alpha}{\sin i\alpha} \equiv v_p \tag{3}$$

- When the spatial axis is aligned with point P, as in Fig. 1-*Right*, we have $t' = 0$ and $\theta = \alpha$. Substituting into (2) yields:

$$\frac{c^2 t}{x} = -ic\frac{\sin i\theta}{\cos i\theta} = -ic\frac{\sin i\alpha}{\cos i\alpha} \equiv v_g \tag{4}$$

Note that these expressions satisfy

$$v_p v_g = c^2 \tag{5}$$

[1]The last step follows from the identities:

$$\cos i(\alpha - \beta) = \cosh(\alpha - \beta) = \cosh\alpha\cosh\beta - \sinh\alpha\sinh\beta$$
$$\sin i(\alpha - \beta) = i\sinh(\alpha - \beta) = i\sinh\alpha\cosh\beta - i\cosh\alpha\sinh\beta$$

and also that, using the identity $\cos^2(i\theta) + \sin^2(i\theta) = 1$, one can isolate the sine and cosine terms in the second case given by Eq. (4) as follows:

$$\cos i\theta = \frac{1}{\sqrt{1 - \left(\frac{v_g}{c}\right)^2}} \equiv \gamma \tag{6}$$

$$\sin i\theta = \frac{iv_g/c}{\sqrt{1 - \left(\frac{v_g}{c}\right)^2}} \tag{7}$$

Moreover, differentiating the invariant spacetime interval $x^2 - (ct)^2 = 1$ with respect to time gives:

$$\frac{dx}{dt} = \frac{d}{dt}\sqrt{(ct)^2 + 1} = \frac{c^2 t}{x} = v_g \tag{8}$$

Thus, by comparing the relations for v_p and v_g with those for the phase and group velocities of an electromagnetic wave V_p and V_g:

$$\begin{array}{l|l} v_p = \dfrac{x}{t} & V_p = \dfrac{\omega}{k} \\ v_g = \dfrac{dx}{dt} & V_g = \dfrac{d\omega}{dk} \\ v_p v_g = c^2 & V_p V_g = c^2 \end{array}$$

we conclude that v_p and v_g are related in precisely the same way as V_p and V_g. Therefore, this demonstrates that the wave-like nature of relativistic phenomena emerges intrinsically from the relationship between space and time as established by special relativity.[2]

3 Geometric Derivation of the Two Fundamental Quantum Properties

In the previous work Ref. [18], we showed that the implicit circular geometry underlying Minkowski rotations is extremely useful for visually deriving various relativistic effects. Although the introduction of the imaginary unit breaks the direct correspondence between Euclidean geometry and the algebraic values of the magnitudes represented within it, the underlying circular structure remains preserved. Practically speaking, this means that we can represent two inertial reference frames as two coordinate systems rotated with respect to one another,[3] and we can also use the sine and cosine of an imaginary angle to make projections in the same manner as with real angles in Euclidean geometry. Through this approach, we were able to geometrically derive time dilation, length contraction, and even gravitational time dilation.

In the present section, we aim to apply the same geometric method to derive the de Broglie and Planck-Einstein relations [28, 39, 40].

3.1 The de Broglie Relation

Consider a rod inside a train car, from which several identical harmonic oscillators are suspended, each oscillating with the same frequency, amplitude, and phase, as illustrated in Fig. 2.

[2]The interpretation of phase velocity in the relativistic context has been historically addressed by de Broglie [28] and further developed in standard quantum treatments [36]. In these frameworks, the phase velocity of matter waves may exceed the speed of light without violating causality, as long as the group velocity—which corresponds to the particle's actual velocity—remains subluminal. While the group velocity is conceptually straightforward and closely tied to observable motion, the meaning of the phase velocity is less intuitive. It does not correspond to the velocity of any physical object, yet it plays a crucial role in the formal structure of wave mechanics. Related geometric approaches have also been explored by Hestenes [37] and Penrose [38], albeit from different foundational principles.

[3]Plus a time reversal effect which corresponds to the -1 in the Lorentzian signature of the metric tensor.

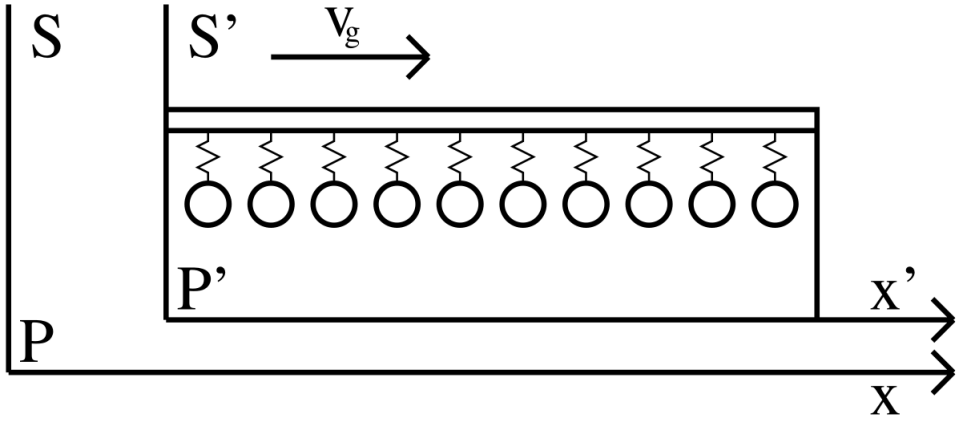

Fig. 2 A train car traveling at velocity v_g with respect to the S-frame. A rod with a set of harmonic oscillators is suspended inside the train. For the observer P' inside the train, the oscillators appear to oscillate in phase with proper frequency f_o. For the observer P on the platform, they appear out of phase due to the relativity of simultaneity and oscillate with a lower frequency f_g due to time dilation.

Louis de Broglie [28] proposed this configuration as an initial representation of a particle with rest mass m_o.[4]

He argued that, when this system is observed from another inertial reference frame (e.g., from the platform, by the observer P), and assuming the relative motion is along the axis of the rod, the oscillators appear out of phase. This phase difference arises due to the relativity of simultaneity. As a result, a *phase wave* emerges along the rod, characterized by a well-defined wavelength λ_p, as shown in Fig. 3.

This wavelength is precisely the one that de Broglie associated with the particle's momentum via the relation

$$p = \frac{h}{\lambda_p},$$

as will be derived in detail below.

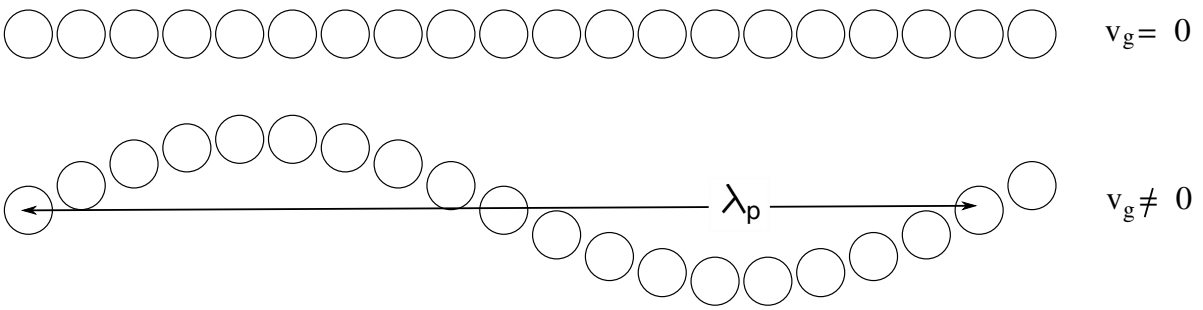

Fig. 3 A rod with hanging oscillators: when at rest with respect to the observer (top), the oscillators appear in phase. When there is relative motion (bottom), the oscillators appear out of phase, generating a phase wave with wavelength λ_p.

The situation illustrated in Fig. 2 can be reinterpreted in terms of rotated coordinate axes, as shown in Fig. 4. In this figure, if we move backward along the t'-axis from the origin by a time interval equal to the proper oscillation period T', we find that the oscillator labeled F lies on the x-axis. This implies that, at $t = 0$ in the S-frame, both oscillators A and F are simultaneous events. Since they are also in the same vibrational state in S', they must appear in phase in S as well (see Fig. 5).

If oscillators A and F are in phase in the S-frame, while the intermediate oscillators (B, C, D, E) are not, the spatial separation AF as measured in S must correspond to the wavelength

[4]Strictly speaking, de Broglie considered a disk with suspended oscillators rather than a rod.

of the resulting phase wave. This distance, denoted by L in the figure, is geometrically related to the proper oscillation period T' via the following expression:

$$L \sin i\theta = icT'$$

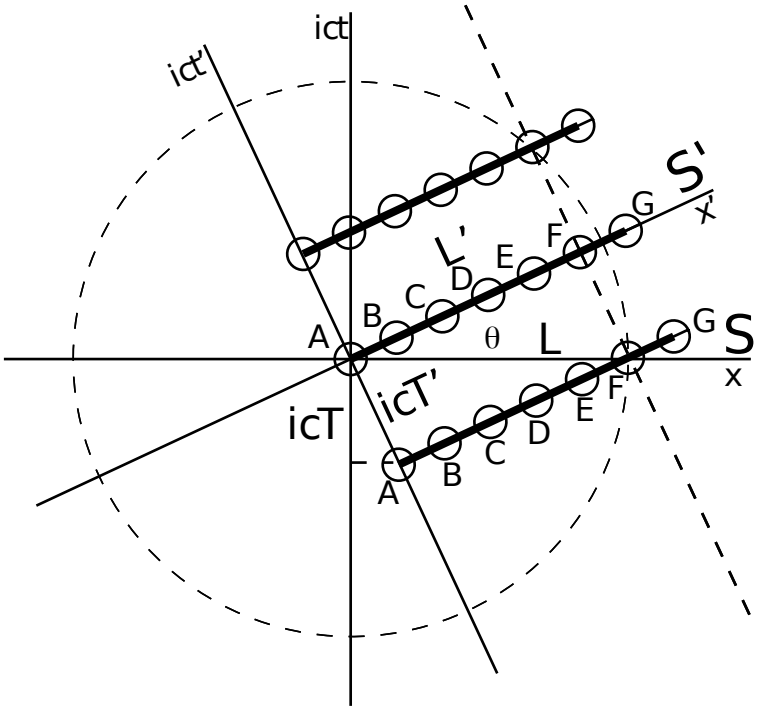

Fig. 4 Two inertial reference frames depicted using the geometric rotation formalism. A rod carrying oscillators A, B, C, D, E, F, ... is at rest in the S'-frame, which moves at velocity $v = -ic\tan i\theta$ with respect to the S-frame. In S', all oscillators oscillate with identical frequency, amplitude, and phase, with proper period T'. The oscillations occur perpendicularly to the plane. The different snapshots along the t'-axis are separated by T', ensuring synchronized oscillations in S'. Note that the angle θ between S and S' is also the angle formed between the rod and the S-frame, so that $\theta = \alpha$.

Therefore, since $L = \lambda_p$, $T' = T_o$, and $\theta = \alpha$, we obtain:

$$\lambda_p = \frac{icT_o}{\sin i\alpha} = \frac{T_o c^2}{v_g}\sqrt{1 - \frac{v_g^2}{c^2}} = \frac{T_o m_o c^2}{p} \tag{9}$$

where identity (7) has been used.

Now, if we define Planck's constant through the relation:

$$hf_o = m_o c^2 \quad \Rightarrow \quad h \equiv T_o m_o c^2 \tag{10}$$

with m_o being the particle's rest mass, we directly recover the well-known de Broglie relation for momentum:[5]

$$p = \frac{h}{\lambda_p} \tag{11}$$

It is important to note that in order to fully justify the definition in Eq. (10), a deeper analysis is required; see section 9 for further discussion.

[5]In the case of light, the de Broglie relation can also be obtained by setting $m_o = 0$ in the energy-momentum relation and using the Planck–Einstein relation $E = hf = hc/\lambda$.

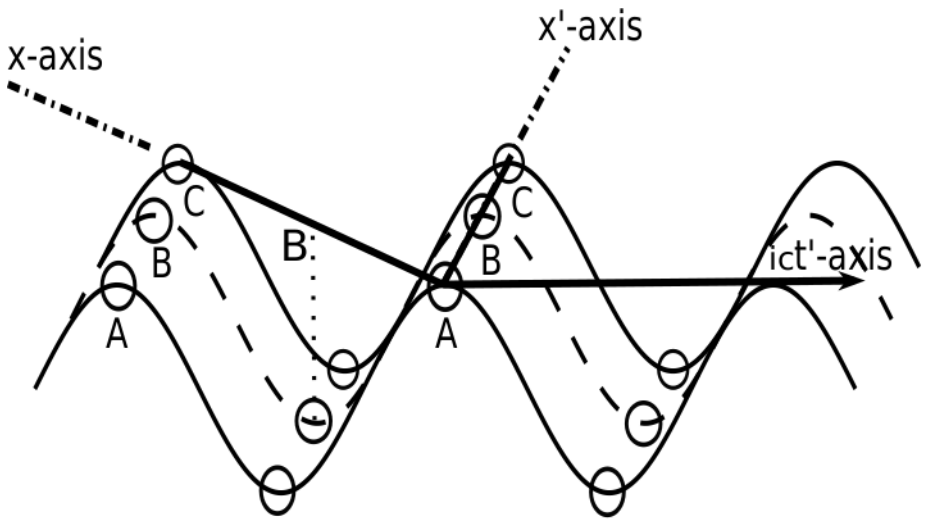

Fig. 5 Alternative view of the rod from Fig. 4, now simplified with only three oscillators: A, B, and C. The rod is at rest in the S'-frame, where the oscillators remain in phase as time t' progresses. However, from the S-frame perspective, due to the angle between the x and x' axes, only the oscillators labeled A and C—which are simultaneous in S—appear in phase, while B is out of phase by π radians. Consequently, the spatial distance AC corresponds to the wavelength λ_p of the phase wave observed in the S-frame.

3.2 The Planck–Einstein relation

The frequency f_p of the phase wave that emerges due to relative motion is given by:

$$f_p = \frac{v_p}{\lambda_p} = \frac{ic\frac{\cos i\alpha}{\sin i\alpha}}{\frac{icT_o}{\sin i\alpha}} = f_o \cos i\alpha \tag{12}$$

where Eqs. (3) and (9) have been used. Multiplying both sides by Planck's constant h and substituting f_o using Eq. (10), we obtain the Planck–Einstein relation:

$$hf_p = m_o c^2 \cos i\alpha = \frac{m_o c^2}{\sqrt{1 - v_g^2/c^2}} \quad \Rightarrow \quad E = hf_p \tag{13}$$

This implies that the energy of a particle at rest originates from the natural frequency f_o of the internal oscillators it comprises. When the particle moves relative to an observer, the frequency associated with its observed energy is not the time-dilated frequency f_g of a single oscillator, but rather the frequency f_p of the phase wave that propagates along the array of oscillators. In this sense, energy arises as a collective, many-body phenomenon.

Let T_g be the oscillation period of a single oscillator as measured from the observer's frame. Due to time dilation, this period transforms as $T_g = \gamma T_o = T_o \cos i\alpha$, yielding the corresponding frequency:

$$f_g = \frac{1}{T_g} = \frac{f_o}{\cos i\alpha}$$

Multiplying this by the expression for f_p in Eq. (12), we obtain an elegant inverse relationship:

$$f_g \cdot f_p = f_o^2 \tag{14}$$

On the spatial side, the distance λ_g traveled by a single oscillator in one period T_g (as measured from S) is:

$$\lambda_g = v_g T_g = v_g \frac{T_o}{\sqrt{1 - v_g^2/c^2}} = -T_o ic \sin i\alpha$$

Comparing this with the phase wave's wavelength λ_p from Eq. (9), we find their product is:

$$\lambda_g \cdot \lambda_p = (-T_o ic \sin i\alpha) \cdot \left(\frac{icT_o}{\sin i\alpha} \right) = c^2 T_o^2 = \frac{c^2}{f_g \cdot f_p}$$

Thus, we obtain:

$$\lambda_g f_g \cdot \lambda_p f_p = c^2 \quad \Rightarrow \quad v_g \cdot v_p = c^2$$

This confirms that v_g corresponds to the physical (group) velocity of the rod or particle, whereas v_p represents the phase velocity associated with the wave resulting from the oscillator's phase displacement.[6]

In summary, interpreting the circular structure as the geometrical foundation of relativity, combined with the model of particles as discrete oscillator chains, allows a natural emergence of wavelike behavior. This framework leads to both key quantum relations—the de Broglie and Planck–Einstein relations—provided the identity $hf_o = m_o c^2$ holds.[7] Importantly, even though no wave packet has been explicitly introduced in this analysis, the velocity of a massive particle behaves as a group velocity. This arises from the fact that, according to the Minkowski rotation, the coordinates x and t are defined over a circular geometry.

4 Particle representation

Figure 6-*1B* shows that, for a specific value of the relative velocity (or, equivalently, of the angle θ) represented in Fig. 6-*1A* (or in Fig. 4), the phase difference between oscillators—forming a particular elementary object modeled as a one-dimensional string of $5 + 1$ oscillators—traces out a regular polygon on a 2π phase wheel.

As the relative velocity between the observer and the rod increases, a new value of θ is reached (see Fig. 6-*2A*) for which oscillators A and F are again in phase as observed from the S-frame. The corresponding shape of the phase wave is illustrated on the right (panel 6-*2C*), while the resulting phase wheel now takes the form of a five-pointed star, as shown in Fig. 6-*2B*.

The fact that intrinsic particle properties—such as momentum and energy—arise from the relative phase differences between oscillators suggests that Figs. 6-*2A* and 6-*2B* may be interpreted as representing the same particle in two different energy–momentum states. For a more faithful representation, however, one should imagine the phase wheel in continuous rotation. That is, if the wheel encodes all possible phases of the harmonic oscillations, then—assuming continuous time evolution (which is natural at macroscopic scales)—each oscillator (points A, B, C, ..., F) would undergo Uniform Circular Motion (UCM), as illustrated in Fig. 7.

It is worth noting that only specific values of the relative velocity (or θ) produce polygons or star polygons on the phase wheel. This observation suggests that more general scenarios could be represented as linear combinations of these stationary phase modes.[8]

4.1 Equivalence between the Wheel of Phases and the Spacetime Wheel

At rest, the oscillators are only distinguished by their positions along the rod. However, as soon as relative motion is introduced, space and time begin to intermingle, and the spatial differentiation among oscillators manifests as differences in timing—that is, as a relative phase shift.

[6] It has long been recognized—starting with de Broglie [28] and further elaborated in standard quantum formulations [36, 41]—that the phase and group velocities associated with a relativistic particle exhibit an inverse relationship, encapsulated by the identity $v_p v_g = c^2$. While the group velocity corresponds to the classical velocity of the particle, the phase velocity—often superluminal—has a more abstract interpretation, reflecting the underlying structure of spacetime geometry—essentially circular—rather than the motion of any physical entity.

[7] This approach differs significantly from the alternative derivations previously proposed—most notably by Penrose [38] and Hestenes [37].

[8] For example, via a Discrete Fourier Transform (DFT).

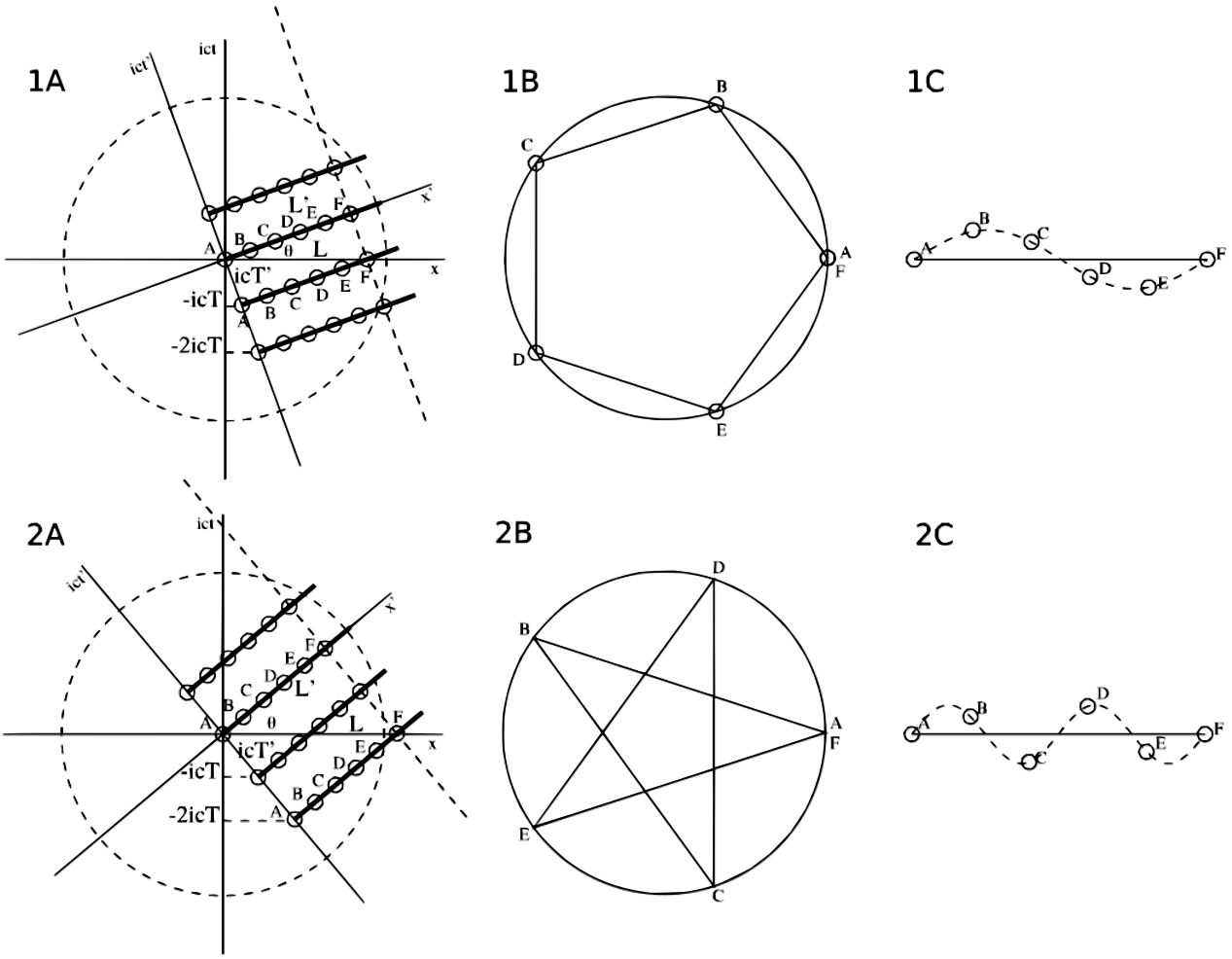

Fig. 6 **Top:** A rod with six oscillators (A to F) in a particular configuration defined by the angle θ. **Bottom:** At a greater value of θ—i.e., at a higher relative velocity—oscillators A and F again oscillate in phase when observed from the S-frame. In this case, the distance $AF = L$ corresponds to two wavelengths. The phase offsets between oscillators form a five-pointed star pattern on the 2π phase wheel, while the corresponding phase wave progression is shown on the **right**.

This suggests that phase itself can be interpreted as a measure of how much time has been converted into space, and vice versa.

Consider, for example, a classical harmonic oscillator at its point of maximum displacement from equilibrium: here, the spatial coordinate (displacement) is maximal, while the velocity is minimal—so minimal, in fact, that successive film frames would appear almost identical, as if time were standing still. Conversely, when the oscillator passes through its equilibrium point, displacement is zero, but velocity (i.e., the indicator of temporal evolution) is maximal, making the motion visibly dynamic from frame to frame, as if time were progressing rapidly. This analogy suggests that harmonic motion can be interpreted as a continuous conversion between space and time—just as uniform circular motion (UCM) in the xy-plane is a continuous transformation of x into y and y into x.

By the same reasoning, each point A, B, C, D, E in Fig. 7 can be viewed as undergoing a dynamic conversion of time into space and vice versa, but each with a relative phase shift. This interpretation justifies the inclusion of spacetime axes in the figure and supports the view that a particle may be understood as a set of discrete points undergoing a spacetime rotation—or equivalently, participating in the fundamental cycle introduced in Ref. [18].

From this perspective, several key conclusions follow:

(i) Since the energy E and momentum p of an elementary object emerge from a collective phenomenon, and this phenomenon can be geometrically represented by a polygon or

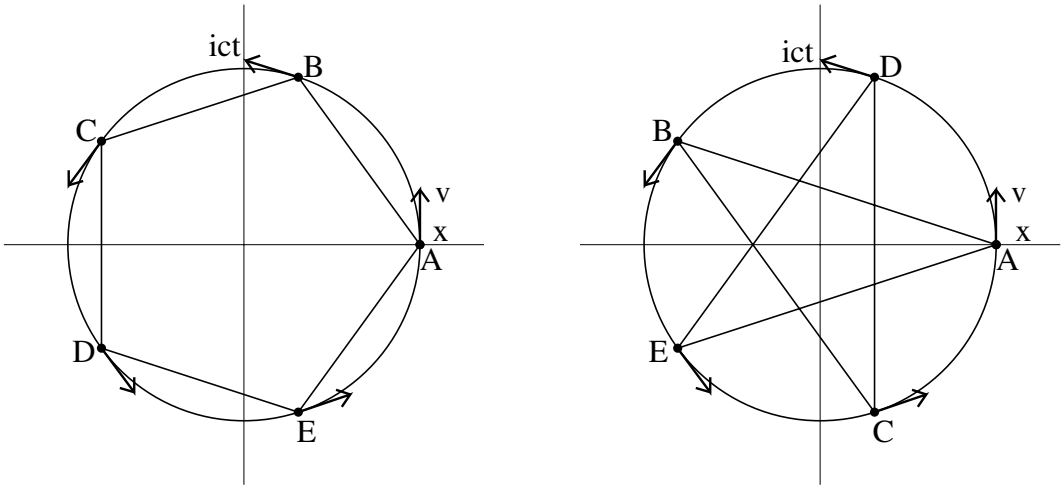

Fig. 7 Illustrates how the phases of the oscillators in Fig. 6 span all possible values via uniform circular motion (UCM), assuming the continuous passage of time, which is appropriate at the macroscopic scale. Since each oscillator undergoes a conversion between time and space, the wheel of phases is effectively a spacetime rotation. For this reason, spatial and temporal axes have been included in the figure.

star polygon inscribed in a phase wheel, such a representation provides an effective and meaningful description of a particle.

(ii) A particle can be conceptualized as a set of discrete points (originally corresponding to de Broglie's oscillators) spinning collectively on a phase wheel.

(iii) We propose that the spinning phase wheel—which encapsulates how spatial differentiation along the rod translates into time delays—is equivalent to a spacetime rotation. This equivalence is of central importance, as it will form the bridge between the microscopic analysis developed in the present article and the macroscopic treatment presented in Ref. [18].

(iv) Since a spacetime rotation constitutes the physical manifestation of the fundamental cycle, elementary particles can be viewed as ensembles of points, each undergoing this fundamental cycle with its own individual phase.[9]

5 The Uncertainty Principle in Relativity

Since the uncertainty principle is deeply tied to wave phenomena, it is reasonable to ask whether it can also be derived from the wave-like nature of relativity discussed in Sections 2 and 3.[10]

Here, we propose a way to do so based on an analogy first described by Feynman [41] between the uncertainty principle and single-slit diffraction. We will show that, within de Broglie's conception of a particle, the scenario arising from relative motion between the observer and the particle resembles that of single-slit diffraction. This analogy allows us to derive, at least to the correct order of magnitude, the uncertainty principle from spacetime properties.

However, for this derivation to hold, the following conjecture—requiring empirical validation—must be satisfied: *just as a diffraction pattern with maxima and minima appears in the single-slit experiment, there must exist certain values of a particle's momentum for which the particle becomes unobservable.*

[9]This representation bears conceptual similarities to earlier discrete or geometrically motivated models, such as spin networks [38, 42], geometric algebra approaches [43], and causal set theory [8]. However, the present framework introduces a distinct construction by associating internal rotational symmetry in spacetime with the different momentum and energy states of a particle.

[10]The uncertainty principle, particularly the position-momentum relation, has historically been understood as a consequence of the wave-like behavior of matter, first introduced by de Broglie [28] and further elaborated in standard quantum frameworks such as Bohm's [36]. In the present work, we offer a distinct derivation of the position-momentum uncertainty relation based on the wave properties emerging from relativistic spacetime structure. This approach diverges from earlier treatments: see Refs. [37, 38].

5.1 Single-Slit Diffraction

In Section 3, we showed that when a rod with hanging oscillators moves relative to an observer, the oscillators appear out-of-phase due to the relativity of simultaneity. The resulting phase distribution takes the form $n\phi$, where $n = 0, 1, 2, 3, ...$ denotes the position of each oscillator along the rod.

A similar phase pattern emerges in single-slit diffraction (see Fig. 8). Imagine n equally spaced oscillators aligned along the slit, all oscillating with the same amplitude but with differing phases due to a time delay introduced by observing them at an angle θ. The phase of each oscillator again takes the form $n\phi$.

The transverse momentum p_y acquired by the particles due to diffraction is typically derived using the two similar triangles shown on the left of Fig. 8. Using the de Broglie relation and the fact that the angle θ corresponds to the first diffraction minimum, where p_y represents the uncertainty Δp, one obtains:

$$\left.\begin{aligned} \lambda &= L\sin\theta \approx L\theta \\ \Delta p = p_y &= p_0 \tan\theta \approx p_0\theta \\ p_0\lambda &= h \end{aligned}\right\} \implies \Delta p \approx \frac{h}{L} \tag{15}$$

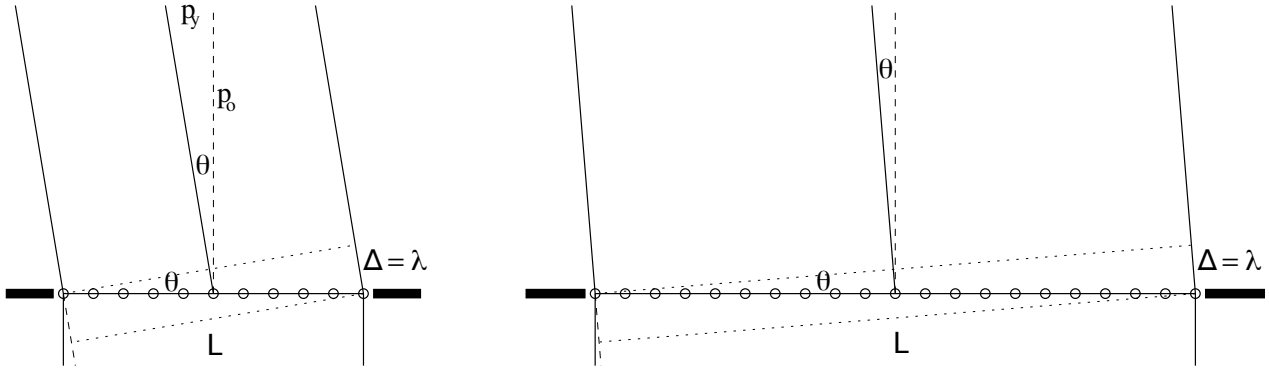

Fig. 8 A beam of particles undergoes single-slit diffraction. According to the Huygens–Fresnel principle, the slit can be modeled as a set of oscillators moving in phase. However, when observed at an angle θ from a far distance (compared to slit width), the oscillators appear out-of-phase due to time delay. When the delay between the first and last oscillators equals one period, the optical path difference $\Delta = vT = \lambda$, resulting in the first diffraction minimum. The left and right images differ in the number of oscillators; as the number increases, the diffraction angle θ decreases, sharpening the diffraction peak and reducing the momentum uncertainty along the slit direction.

If the slit width L is taken as the uncertainty in position Δx, then the product of uncertainties becomes:

$$\Delta x \cdot \Delta p \approx L \cdot \frac{h}{L} = h \tag{16}$$

This relationship is visually intuitive in Fig. 8: as the number of oscillators increases, the angle θ narrows. Conceptually, this forms a right triangle with a fixed leg λ (the wavelength), and as the hypotenuse (representing Δx) increases, the angle—and hence Δp—decreases.

5.2 The Phase Wave in Single-Slit Diffraction

An equivalent analysis can be made by considering the diffraction effect as arising from a phase wave observed along the line of oscillators.

As seen in Section 3.1, the wavelength λ_p of the phase wave was associated with the particle's momentum through $p = h/\lambda_p$, where the phase wave itself emerged due to the relative motion between rod and observer.

In the single-slit case, we observe a similar phase wave even though there is initially no relative motion—unless one interprets the diffraction itself as arising from such motion. In other words, could the observed phase wave in the slit be what gives rise to relative motion between the slit and the diffracted particles along the slit direction?

Assuming this hypothesis, the phase wave itself would be responsible for the diffraction effect. In the setup shown in Fig. 8, for the first minimum (angle θ), we know that the phase wave's wavelength is:

$$\lambda_p = L\cos\theta \approx L$$

Then, the corresponding transverse momentum becomes $p_y = h/\lambda_p \approx h/L$, matching the result in (15). This consistency supports the idea that the diffraction mechanism may indeed be a manifestation of the phase wave along the oscillator line.

Extending this interpretation, we can analyze the diffraction pattern beyond the central peak. Fig. 9 illustrates the phase waves—within a line of 5+1 oscillators—that result in maxima and minima between the first two strong diffraction peaks. The waves labeled 0 and 1 contribute to the strong central maximum ($\theta \approx 0$), while wave 2 marks the first minimum. Subsequent weak maxima appear for waves 3, 5, and 7, and waves 9 and 10 correspond to the next strong maximum. Strong maxima occur when all oscillators are in phase (or nearly so), whereas in weak maxima, phase contributions mostly cancel except for one residual peak.

In summary: - Maxima correspond to an accumulated out-of-phase equal to an odd multiple of π. - Minima occur when the accumulated out-of-phase equals a multiple of 2π.

Each phase wave in Fig. 9 is represented both in a 2π-radian wheel (left) and a π-radian wheel (right). From their shapes, the minima satisfy $\lambda = L/m$, where $m \in \mathbb{N}$. Consequently, the uncertainty in momentum associated with each minimum increases by a factor m, yielding:

$$\Delta x \cdot \Delta p = mh \tag{17}$$

Thus, Eq. (16) corresponds to the minimum bound of the uncertainty.

5.3 The Uncertainty Principle in Spacetime

A situation analogous to the single-slit diffraction occurs when a rod with hanging oscillators is observed in relative motion: as illustrated in Fig. 10, increasing the number of oscillators (from left to right) leads to a decrease in the angle θ, similarly to the behavior seen in the diffraction pattern. In this case, the right triangle formed has a leg corresponding to the proper oscillation period icT', and a hypotenuse corresponding to the observed rod length L.

For the particular configurations shown in the figure, the wavelength of the phase wave λ_p is equal to the rod length L as measured by the observer. Therefore, the associated momentum is given by $p = h/L$, analogous to Eq. (15). However, can this value of p now be interpreted as a measure of the momentum uncertainty Δp? In other words, does this particular angle θ correspond to a form of minimum, as in the case of diffraction, where a minimum emerges from destructive interference between all oscillators? By analogy, could the rod (i.e., the particle) become unobservable for a specific relative velocity or angle?

Let us assume this to be the case—that is, the momentum $p = h/L$ corresponds to a kind of minimum and can be taken as a measure of the uncertainty $\Delta p = h/L$. If we now identify the observed rod length L with the uncertainty in position Δx, this leads again to the same result as in Eq. (16):

$$\Delta x \cdot \Delta p \approx h$$

This suggests the following:

- *In order to derive the uncertainty principle from the properties of spacetime, one must assume that whenever the wavelength of the phase wave satisfies the condition $m\lambda_p = L$, a minimum occurs, whatever the precise physical interpretation of this minimum might be.*

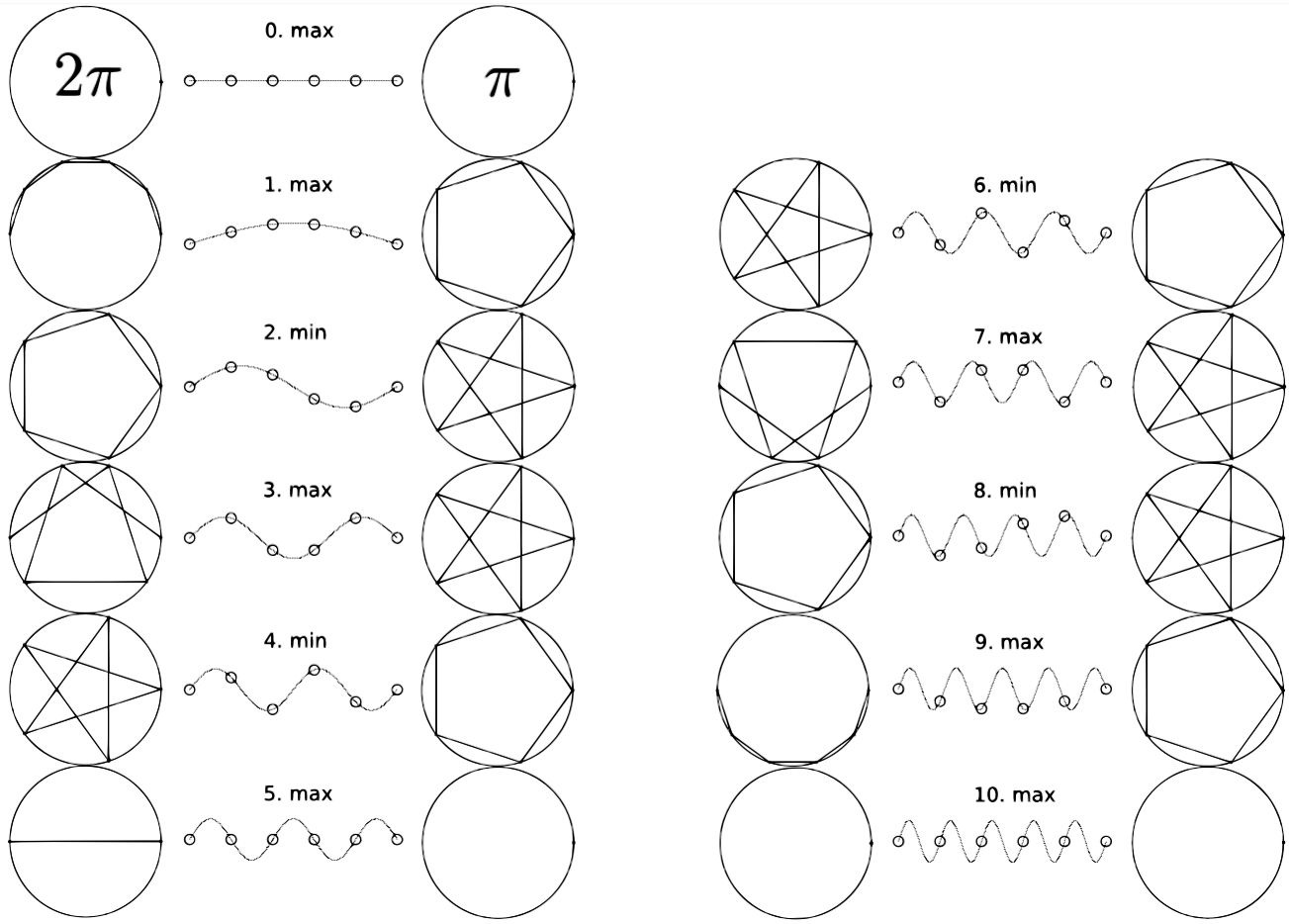

Fig. 9 Phase waves (between the first two strong diffraction peaks) for a slit with $5+1$ oscillators. The left side of each wave shows the out-of-phase in a 2π wheel; the right side in a π wheel. Open paths in the 2π representation correspond to maxima, while closed paths correspond to minima.

Although Eq. (16) appears valid in both the diffraction and rod scenarios, there are significant physical differences between the two cases. In the single-slit diffraction, the slit width as observed at an angle θ is $L' = L\cos\theta$, implying a contraction: $L' < L$, since $\cos\theta < 1$. In contrast, in the relativistic case, the observed rod length is $L = L'/\cos i\theta$, which also leads to contraction ($L < L'$), as $\cos i\theta > 1$. However, the contraction factor differs in both scenarios, as $\cos\theta \neq (\cos i\theta)^{-1}$. Nevertheless, for the uncertainty relation $\Delta x \cdot \Delta p$, this distinction is immaterial, since L cancels out in the product.

Let us now identify the specific situations in which a maximum or a minimum is realised:

Both cases of relative motion between the observer and the particle, as shown in Figs. 6-*1A* and *2A*, correspond to minima, since they are associated with closed paths in a 2π-radian phase wheel, as depicted in Figs. 6-*1B* and *2B*. The same applies to the cases shown in Figs. 11-*3A* and *4A* (which correspond to phase waves 6 and 8 in Fig. 9): all of them correspond to minima.

As the angle θ continues to increase, one reaches a maximum, as illustrated in the central image of Fig. 12, where all oscillators are once again in phase—mimicking the behavior of the rod at rest.

However, between any two minima, there exist maxima. The corresponding phase waves are configurations 3, 5, 7, and 9 in Fig. 9.

Therefore, in the specific case of a rod with $5+1$ oscillators, there exist ten distinct phase wave configurations that lead either to a maximum or a minimum. Among these ten configurations, five correspond to maxima and five to minima. As previously noted, the minima might be associated with conditions under which the particle becomes unobservable. In contrast, it will be shown in Section 9 that it is more convenient to represent maxima in a π-radian phase

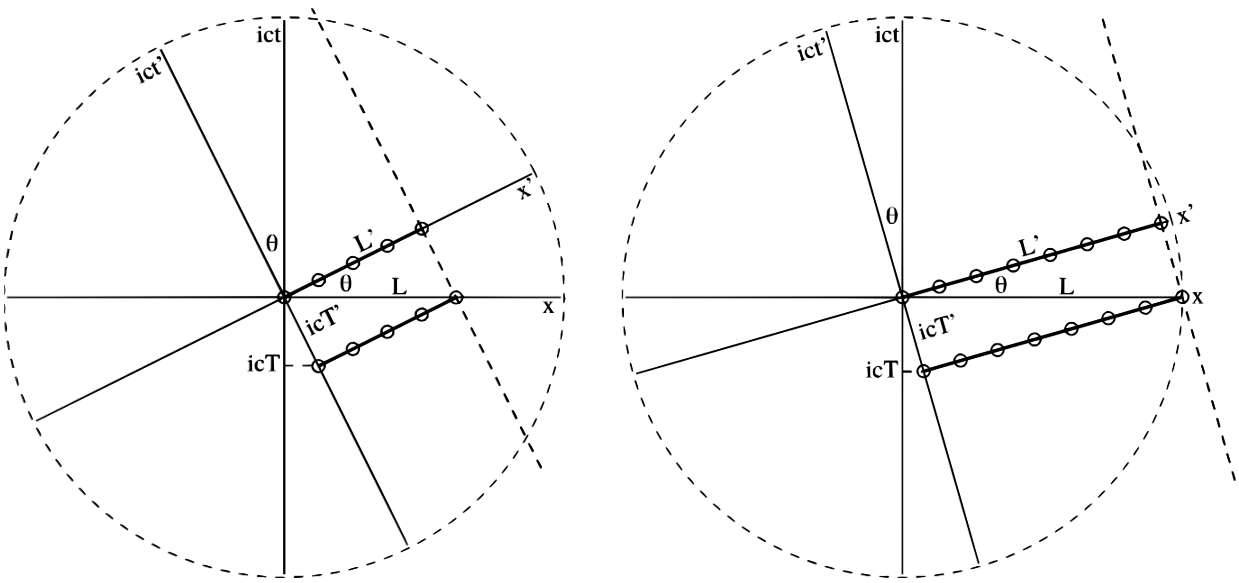

Fig. 10 **Left:** A particle (represented as a rod with $4+1$ hanging oscillators) is shown at rest in the S' frame. This frame is moving at a velocity $v = -ic\tan i\theta$ with respect to the S frame, such that the observer perceives the first and last oscillators as oscillating in phase. **Right:** The number of oscillators has been increased from 5 to 8, which results in a narrower angle θ for the same proper oscillation period T'.

wheel instead of a 2π-radian one. This approach enables a direct determination of a particle's spin based on its circular representation. In this context, Fig. 13 displays all the maxima corresponding to those configurations where a particle composed of $5+1$ oscillators becomes observable.

From this analysis, several conclusions can be drawn:

(i) Assuming de Broglie's interpretation of a particle as a discrete string of oscillators, the uncertainty principle in spacetime can be derived in order of magnitude by analogy with single-slit diffraction.

(ii) Nevertheless, for the analogy to be complete, one condition must be satisfied: just as diffraction patterns exhibit minima, spacetime must also allow for particular relative velocities — or equivalently, momenta — at which the particle becomes unobservable. This hypothesis remains to be tested experimentally.

(iii) Conversely, there are also momenta for which the particle exhibits maxima, analogous to the bright fringes in a diffraction pattern. These maxima, which might correspond to the only observable configurations, are represented as closed paths forming either a polygon or a star polygon in a π-radian phase wheel. Thus, the circular representation of particles proposed in Section 4 should henceforth be associated exclusively with π-radian phase wheels, in order to exclude those unobservable configurations corresponding to minima.

6 Discrete spacetime

In Section 3, the concept of an elementary particle was understood as a set of elements—originally conceived as oscillators—undergoing their own fundamental cycle, namely, a spacetime rotation. Moreover, as shown in Ref. [18], this same framework also served as a cosmological model within the harmonic interpretation of relativity.

This dual applicability suggests that the proposed concept of particle may unify both microscopic and macroscopic regimes. However, this model is based on two key assumptions: (1) the validity of the relation $hf_o = m_o c^2$, and (2) the description of a particle as a discrete string of oscillators. The aim of the following sections is to justify both assumptions.

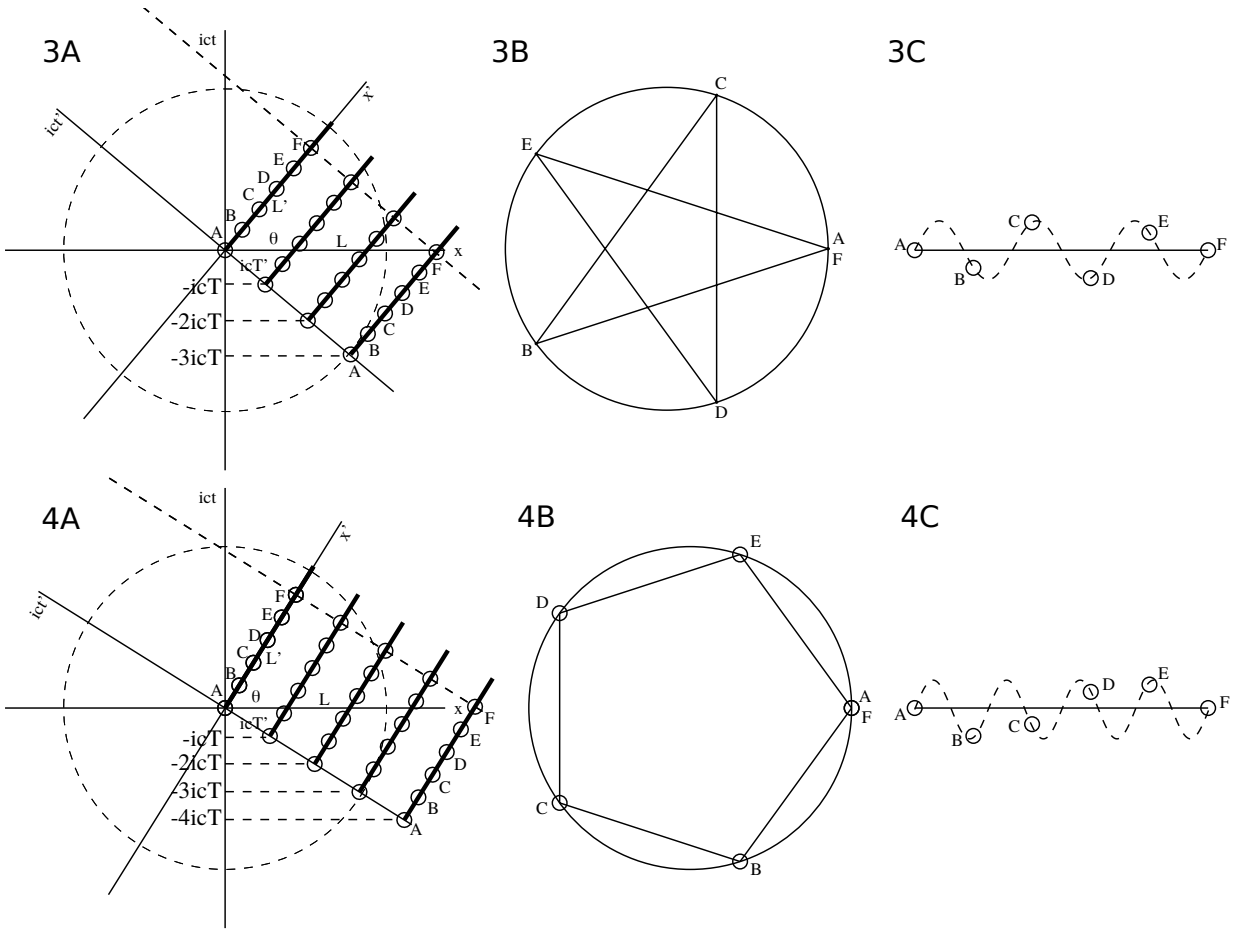

Fig. 11 **3A:** Another value of θ for which oscillators A and F are seen oscillating in phase in the S frame; now the distance between them is $AF = L = 3\lambda_p$. **3B:** The out-of-phase is $3 \cdot 2\pi/5$ radians, forming a five-pointed star rotating clockwise. **3C:** Passage of the phase wave. **4A:** The next angle for which A and F oscillate in phase; now $AF = L = 4\lambda_p$. **4B:** The out-of-phase is $4 \cdot 2\pi/5$, yielding another pentagon also rotating clockwise. **4C:** Passage of the phase wave.

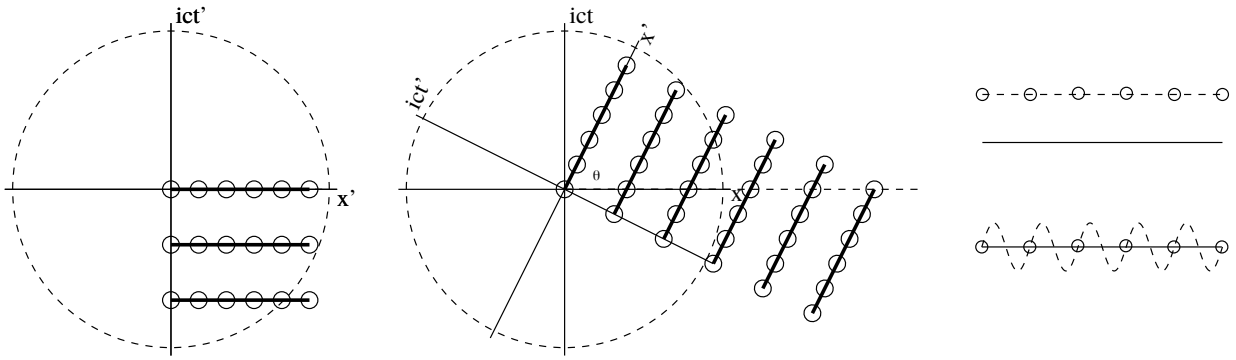

Fig. 12 The spacetime diagram on the left shows the rod at rest, with all oscillators oscillating in phase as depicted in the top-right corner. The central image demonstrates that there exists a particular angle θ for which the oscillators come back into phase, as shown in the bottom-right image (note that the fact $\theta > \pi/4$ is not essential here).

To this end, we shall adopt a microscopic approach by addressing a fundamental question: what is the true nature of time? [11] To explore this, we shall consider a system of interacting elements and enumerate all possible configurations in which these elements may be either

[11] For alternative perspectives on the nature of time, see Refs. [44–47].

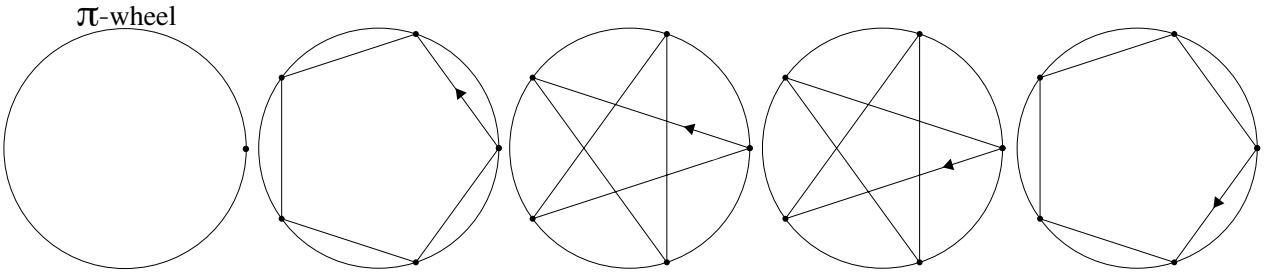

Fig. 13 Displays the five distinct phase configurations in a π-radian phase wheel corresponding to the maxima associated with cases 0 (also 5 and 10), 1, 3, 7, and 9 in Fig. 9. These are considered the only stationary configurations in which a particle composed of $5+1$ oscillators may be detected, under the assumption that minima correspond to unobservable states — by analogy with diffraction minima.

present or *absent* at a given stage.[12] These possibilities, or elementary events, will then be arranged in sequence to define a notion of timeline.

Next, we shall assign algebraic values to these events: real values for presence and imaginary values for absence (and vice versa), resulting in a complex representation of time. In this framework, the evolution of the timeline will trace out a discrete circular motion in the complex plane. This motion will then be interpreted as the discrete analogue of the spacetime rotations previously introduced in Ref. [18].

In addition, two distinct types of solutions will emerge from this analysis: one that appears *locally linear*, and another that is clearly *rotational*. We shall propose that the linear solution is associated with the "group" properties of matter, while the rotational one corresponds to its "phase" characteristics. Since these two behaviors mirror the dual nature of wave and particle, the identity $L\omega_o = m_o c^2$ will be introduced. The task of demonstrating that $L = \hbar$ will be addressed in Section 9.

On the other hand, we will see that conceiving a particle as a discrete line of oscillators—originally suggested by de Broglie—is conceptually equivalent to assuming a discrete structure of spacetime.

6.1 Definition of Event

Consider an interaction set composed of N distinct elements. For the time being, we are not concerned with the specific nature of these elements or the details of their interactions. Rather, our sole interest lies in counting the number of distinct configurations in which these elements may be either *present* or *absent* at a given stage. Each such configuration will be referred to as an *event*, or equivalently, an *interaction*.

- In the case of a zero-element interaction set, $N = 0$, there exists only one possible configuration: the empty stage (Fig. 14).
- For an interaction set with a single element, $N = 1$, there are exactly two possible events: either the element (labeled A in Fig. 15) is present, or it is absent.

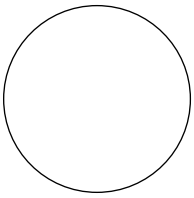

Fig. 14 The only possible event or interaction in a set with zero elements: an empty stage.

[12] Note that this constitutes a discretization of the concepts of presence and absence introduced in Ref. [18] at a macroscopic level.

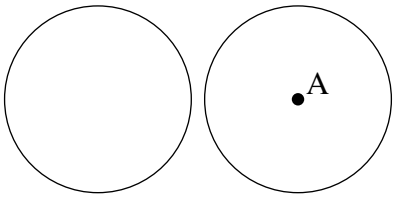

Fig. 15 The two possible events in a one-element interaction set.

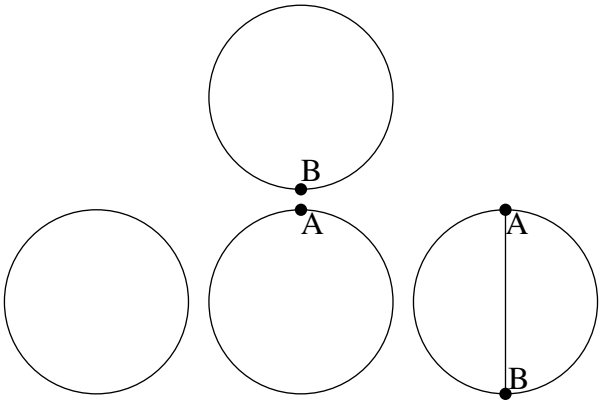

Fig. 16 The four possible events in a two-element interaction set, distributed in columns according to the number of elements present in each event.

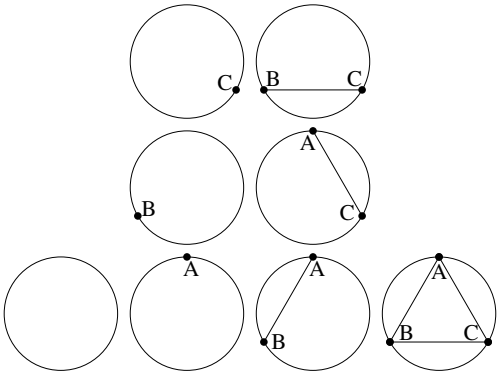

Fig. 17 The eight possible events in a three-element interaction set.

- In a set containing two elements, $N = 2$, say A and B, there are four distinct events, as illustrated in Fig. 16. These are arranged in columns as $1 + 2 + 1$, indicating one event with zero elements (the void), two events with a single element, and one event involving both elements. Note that the total number of events is given by 2^2, where the exponent denotes the number of elements in the set.
- For $N = 3$, the total number of events is $2^3 = 8$ (Fig. 17), which can be grouped according to the number of elements present in each configuration as $1 + 3 + 3 + 1$. These values correspond to the binomial coefficients in Pascal's triangle (Fig. 18).
- Accordingly, in a four-element interaction set, the total number of events is $2^4 = 16$, which are distributed as $1 + 4 + 6 + 4 + 1$. This can be verified in Fig. 19.

From the above, we may conclude the following:

- *The number of events in an interaction set with N elements is given by 2^N, and these events are distributed—according to the number of elements involved in each event—in correspondence with the N^{th} row of Pascal's triangle.*

1
1 1
1 2 1
1 3 3 1
1 4 6 4 1
1 5 10 10 5 1
1 6 15 20 15 6 1
1 7 21 35 35 21 7 1

Fig. 18 Pascal's triangle displays the binomial coefficients, which among many other properties, provide the distribution—by number of participating elements—of all possible events within sets containing 0, 1, 2, 3, ... elements.

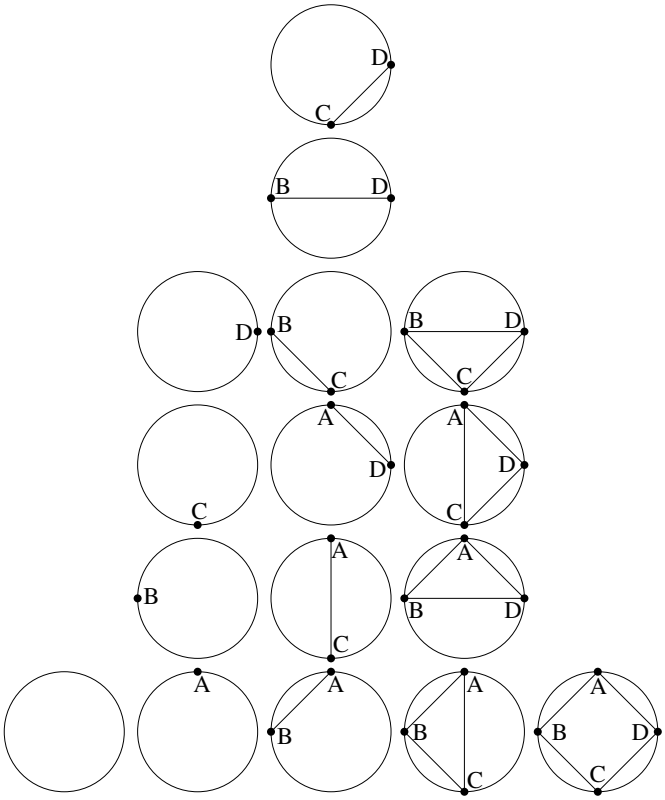

Fig. 19 The sixteen possible events in a four-element interaction set.

6.2 The Timeline

We now aim to arrange the 2^N possible events of an N-element interaction set into a sequence, in the hope of unveiling the structure of the timeline.

To approach this, let us begin by asking: what is the nature of time?

It has been said that *"time is what happens when nothing else happens"* [41]. Although insightful, this definition does not provide a practical means of measuring time. In practice, time is measured through events: *from the motion of celestial bodies to the ticking of a mechanical clock, or the vibration of atoms or molecules.* These are all events that occur with a certain periodicity. Yet, if we limit ourselves solely to periodic phenomena, we risk overlooking a fundamental characteristic of time: the fact that it never repeats. Therefore, for our present purposes, time will be understood as *a cyclic sequence of events that never exactly repeats.*

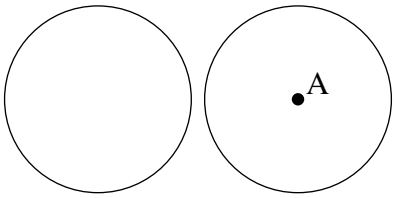

Fig. 20 The two events in a one-element interaction set, arranged from left to right according to their temporal sequence.

If the 2^N possible events within an N-element interaction set were to occur temporally, what would be their natural order? Is there a consistent method to arrange them in sequence? If such a method exists, uncovering it would likely provide insight into the very mechanism behind temporal evolution itself.

- The simplest case is the 0-element interaction set. Since it contains only a single event—the void—there is nothing to order.
- The 1-element interaction set contains two events (Fig. 20). Here, two sequences are possible: either the void comes first, or second. It seems reasonable to assign priority to the void, since it was the only state present in the 0-element case.
- The 2-element interaction set includes four possible events:
  - The void,
  - Only element A is present,
  - Only element B is present,
  - Both A and B are present.

  In total, there are $4! = 24$ possible permutations. However, by assigning the void to the first position, we reduce this to $3! = 6$. Furthermore, since the event where both A and B are present must occur last—so that neither appears prematurely—we are left with only two valid sequences. To avoid ambiguity, we simply define the first element to enter the stage as A[13], yielding the timeline shown in Fig. 21.

  Note that the first two events of this timeline match those in Fig. 20, and that the void again occupies the first position. This suggests a recursive structure: *the first half of the new timeline corresponds to the entirety of the previous one.*

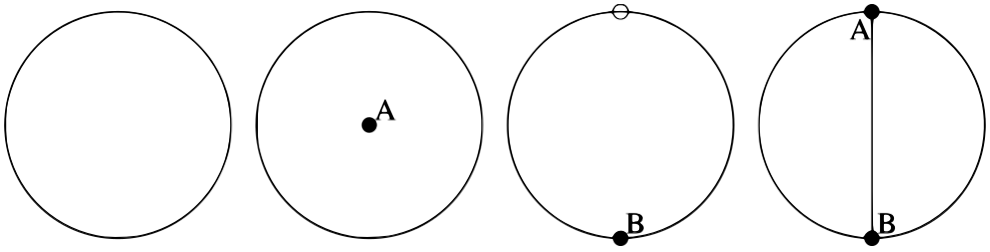

Fig. 21 The timeline in a two-element interaction set, ordered from left to right. Note that the first two events reproduce those in Fig. 20.

- If the recursive hypothesis holds—that *the first half of a timeline equals the full previous timeline*—then the timeline of a 3-element interaction set should begin with the 4 events shown in Fig. 21. The fifth event must then introduce the new element C, since the cycle of A and B is complete. The simplest option is to add C alone. To maintain a non-repeating cyclic structure, C must remain present while A and B re-enter by repeating their earlier sequence. This yields the timeline illustrated in Fig. 22.

  This suggests a clear recursive construction rule:

[13]This combinatorial decision may be revisited in future work where a broader generalization is required.

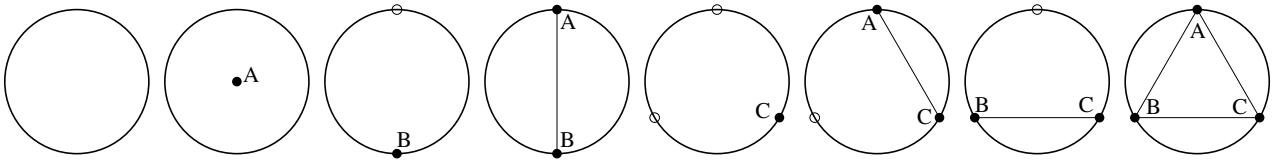

Fig. 22 The eight possible events in a three-element interaction set, arranged in temporal sequence from left to right.

	D	C	B	A
1	0	0	0	0
2	0	0	0	1
3	0	0	1	0
4	0	0	1	1
5	0	1	0	0
6	0	1	0	1
7	0	1	1	0
8	0	1	1	1
9	1	0	0	0
10	1	0	0	1
11	1	0	1	0
12	1	0	1	1
13	1	1	0	0
14	1	1	0	1
15	1	1	1	0
16	1	1	1	1

Table 1 Shows the absence (0) and the presence (1) of each element A, B, C and D in each step in the timeline obtained in Fig. 23. Notice that it is the binary code.

  - *Whenever the interaction set is increased by one element, the new timeline is formed by concatenating the previous timeline with a duplicate of it, in which each event includes the newly added element.*
- Fig. 23 shows the result of applying this method to a 4-element interaction set.

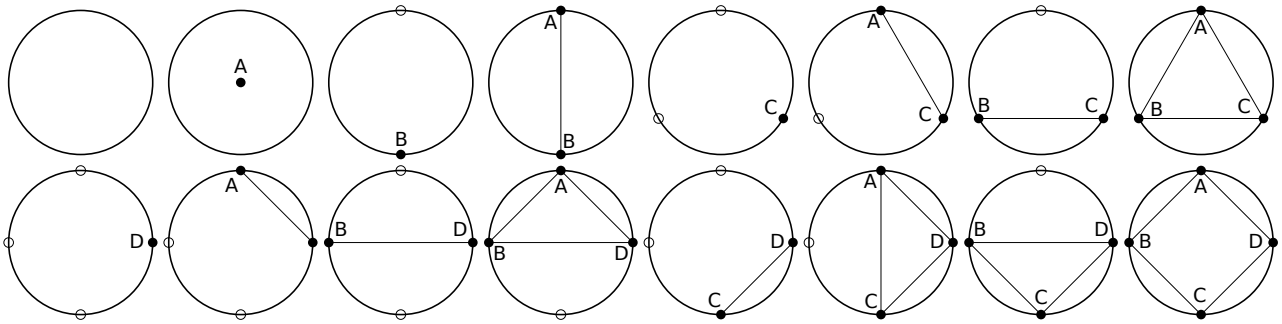

Fig. 23 The 16 possible events in a four-element interaction set involving A, B, C, and D, arranged in temporal order from left to right and top to bottom.

A closer look at the timeline in Fig. 23 reveals an intriguing pattern. The presence of element A alternates: $0, 1, 0, 1, 0, 1, 0, 1, \ldots$ where 0 denotes absence and 1 presence. Element B follows the pattern $0, 0, 1, 1, 0, 0, 1, 1, \ldots$ and similarly for C and D. Compiling these patterns into rows yields Table 1, which is none other than the binary number system.

Thus, the recursive timeline construction corresponds to the binary counting sequence, which—true to our definition—has a cyclic nature and never repeats identically.

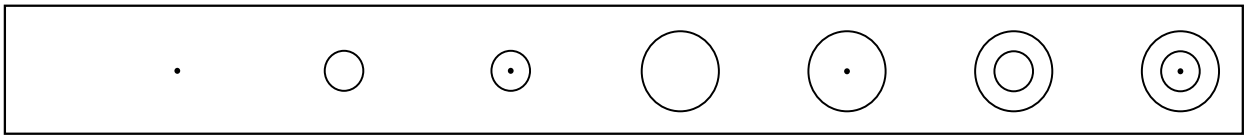

Fig. 24 The three-element timeline previously shown in Fig. 22, now represented from left to right using nested shells. The first event corresponds to the void, for which no shell is drawn.

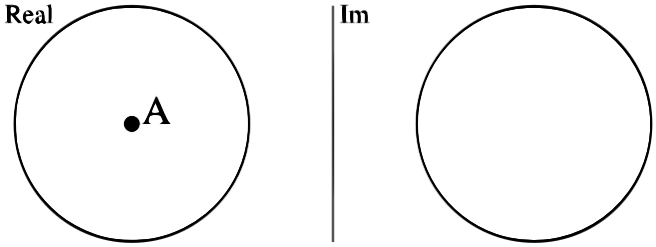

Fig. 25 The two possible events in a 1-element interaction set, classified according to the presence or absence of the element A.

6.3 The Nature of the Elements

The existence of a recursive mechanism for constructing the timeline implies that time is built upon what has already occurred: new elements are introduced only once all combinations of the existing ones have been exhausted.

This observation reveals something fundamental about the elements themselves: it is as if each element is nothing more than a shell—or a container—that encapsulates a cycle of possibilities.

Each new container, once introduced, can interact with all previously created elements. In this sense, the timeline itself appears to generate the elements. Rather than being pre-existing entities, elements are created through the unfolding of temporal sequence.

Since the timeline is a succession of events occurring in time, the elements may be interpreted as distinct instants. Indeed, the emergence of a new element marks a particular moment in which the full diversity cycle of the previous elements has completed, and it becomes possible to fold that cycle into a compact structure—a new element. As will be demonstrated in Section 7, this folding admits a precise mathematical formulation,[14] whereby those moments with a single element on stage are the only ones that can be expressed in a compact algebraic form.

Visualising each element as a shell enclosing the prior cycle of possibilities evokes the image of nested boxes, akin to the structure of *Russian matryoshkas*. Accordingly, the timeline can be represented in terms of shells. Figure 24 illustrates the timeline from Fig. 22 in this alternative representation. This shell-based depiction adds accuracy by making the relative sizes of the elements explicit.

6.4 Real and Imaginary

We are now in a position to adopt an internal perspective within the system. To this end, let us imagine ourselves as one of the elements, say the A-element. As we shall see, by including ourselves within the structure, two distinct sets naturally emerge—referred to as the *Real* and the *Imaginary* sets—which endow each element with a tangible/intangible—or presence/absence—duality. Algebraically, this duality will be captured in the following section by means of complex numbers.

In Section 6.1, interaction sets composed of multiple elements were analysed. It was established that an interaction set with N elements yields a total of 2^N possible events.

Let us now classify the events in Figs. 15, 16, and 17 based on the presence or absence of the A-element. The result is illustrated in Figs. 25, 26, and 27, respectively. Observe that in

[14] See expression (18).

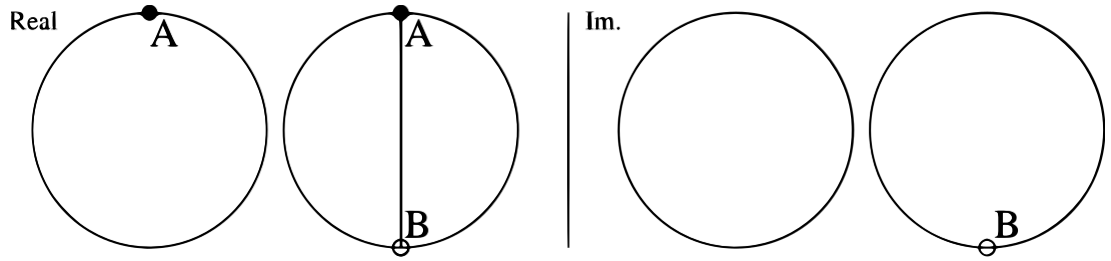

Fig. 26 The four possible events in a 2-element interaction set, classified according to the presence of the element A. Note that both Real and Imaginary sets are arranged in columns following the binomial coefficients $1+1$.

each case, the A-element (or any other element, by analogy) is present in exactly half of the total number of events. Furthermore, these events are distributed according to the $(N-1)^{\text{th}}$ row of Pascal's triangle.

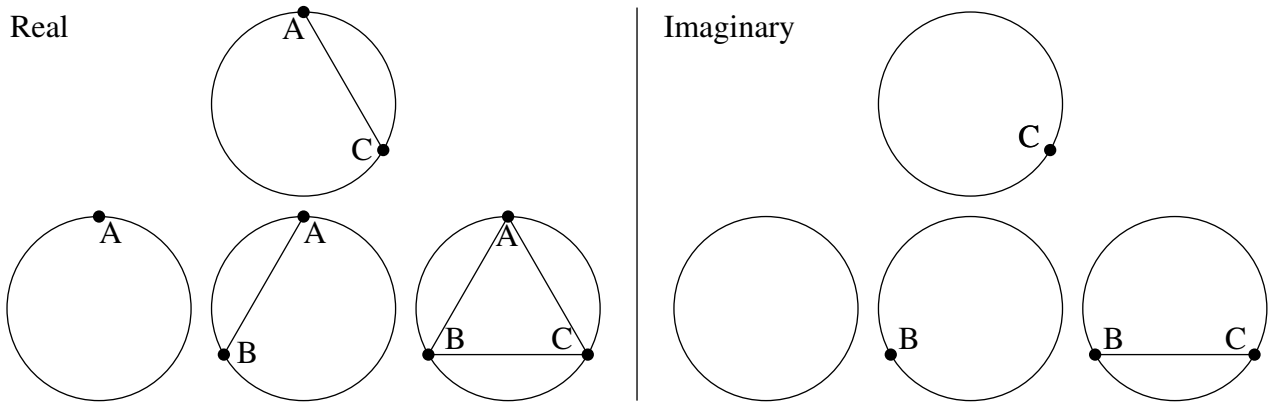

Fig. 27 The eight possible events in a 3-element interaction set, classified according to the presence or absence of the A-element.

Hence, one can already anticipate that in a 4-element interaction set, the A-element will appear in 8 out of the total 16 events. These events will be distributed according to the binomial coefficients $1+3+3+1$, as can be verified in Fig. 19. Similarly, the remaining 8 events in which A is absent will follow the same distribution.

7 The timeline values

Let us reproduce the timeline from Fig. 22 as Fig. 28. The goal now is to assign to this timeline an algebraic value—that is, to derive its algebraic expression as a function of the number of elements N. Representing the timeline as a function of N effectively means expressing the passage of time, since each element is assumed to be generated by the timeline itself. Henceforth, the number of elements N will no longer be regarded as a fixed constant, but rather as a variable that increases over time. Accordingly, we will denote it simply by n.

As discussed in the previous section, each element perceives the system in a unique dual fashion—*Real* and *Imaginary*—and this duality must be accounted for in any self-referential description of the system. Therefore, we now introduce complex numbers in the following manner:

(i) A complex number is assigned to each event.
(ii) The total value of the timeline is obtained by summing the values of all individual events.
(iii) A value a is assigned to the empty stage.
(iv) A value b is assigned to any event consisting of a single element. This value b can be interpreted as a kind of probability amplitude for a single-element event.

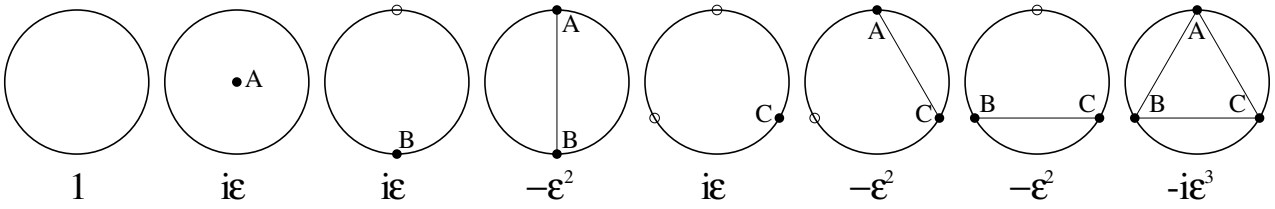

Fig. 28 The timeline for a 3-element interaction set. Below each event is its corresponding value, given by $(i\epsilon)^m$, where m is the number of elements participating in the event.

(v) Events with two or more elements on stage are interpreted as superpositions of multiple single-element events. Therefore, their amplitude is the product of m such amplitudes, i.e., b^m.

(vi) The timeline always begins with the empty stage, and is followed by the appearance of the first element. This transition from emptiness signifies the emergence of a new kind of entity. Consequently, when assigning values to a and b, they are required to be of opposite mathematical nature: if a is purely imaginary, then b must be purely real, and vice versa.

(vii) The modulus of a is normalized to 1, since for $n = 0$, the empty stage is the only possible event. That is, $a^*a = 1$.

(viii) The modulus of b should reflect the fact that n different elements may be involved, although its exact dependence on n remains unknown. What can be asserted is that the modulus of b is expected to decrease as n increases. As a first approximation, it is assumed that b is very small for $n \gg 1$, and will therefore be denoted as ϵ.

These considerations leave us with two distinct options:

1. $a = 1, \quad b = i\epsilon$
2. $a = i, \quad b = \epsilon$

7.1 First Option: a = 1 and b= iϵ

Applying the first option to the timeline in Fig. 28, we obtain the values shown beneath each event in the figure. Here one could argue that it would be more natural to associate an imaginary number with each absent element, since it is absence—not presence—that we previously related to imaginary numbers [18]. However, note that due to the symmetry between presence and absence along the temporal line, we would have obtained exactly the same result.

To determine the total value of the timeline, we sum all these individual contributions:

$$1 + i\epsilon + i\epsilon + (i\epsilon)^2 + i\epsilon + (i\epsilon)^2 + (i\epsilon)^2 + (i\epsilon)^3 = 1 + 3i\epsilon + 3(i\epsilon)^2 + (i\epsilon)^3 = (1 + i\epsilon)^3$$

or more generally:

$$(1 + i\epsilon)^n \tag{18}$$

where n denotes the number of elements in the interaction set.

Since incrementing n corresponds to the forward passage of time, let us refer to such discrete temporal progress as the *tick of time*.

Graphically representing this expression for increasing values of n, as shown in Fig. 29, yields a discrete rotation along the unit circle in the complex plane. The smaller the value of ϵ, the closer the plotted values lie to the unit circle, and the more densely they are distributed. In the limit $\epsilon \to 0$, the curve converges to a perfect circle. Furthermore, by projecting this circular motion onto the real and imaginary axes for increasing n, one obtains the curves shown in Fig. 30, identified respectively as the *algebraic cosine* and *algebraic sine*.

Expression (18) becomes particularly significant when ϵ is small, since the term in parentheses may then be approximated by the exponential $e^{i\epsilon}$:

$$(1 + i\epsilon)^n = \left(e^{i\epsilon}\right)^n \tag{19}$$

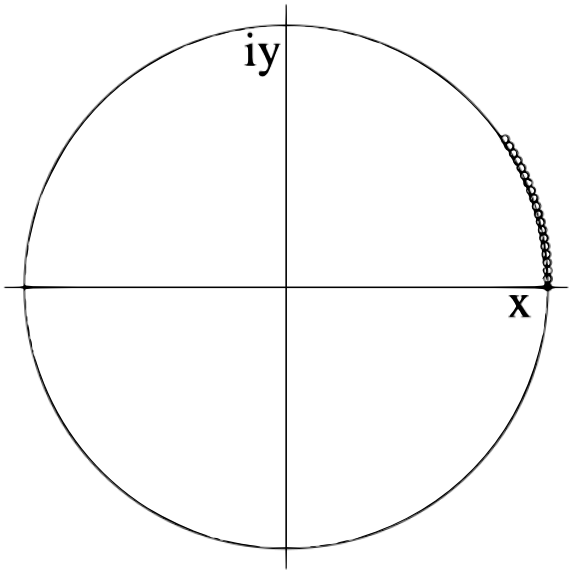

Fig. 29 Graphical representation of $(1 + i\epsilon)^n$ for $\epsilon = 2^{-5} = 0.03125$ and varying n values ($n = 0, 1, 2, \ldots, 20$). The slight deviation from the unit circle arises from the relatively large value of ϵ.

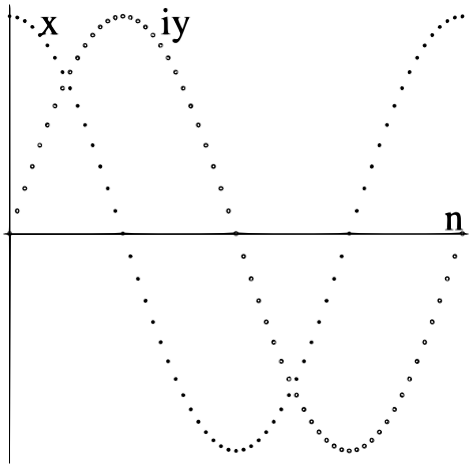

Fig. 30 Displays the real and imaginary parts of $(1 + i\epsilon)^n = \cos(n\epsilon) + i\sin(n\epsilon)$ for fixed ϵ and increasing n.

Therefore, the first solution for the timeline represents a discrete uniform circular motion (UCM) in the complex plane—essentially a discrete version of the spacetime rotations first introduced in [18].

7.2 Second Option: a = i and b = ϵ

This second option does not permit assigning a distinct value to each individual event and then summing them to compute the total value of the timeline. Nevertheless, due to symmetry considerations, the overall value of the timeline is expected to retain a compact form similar to expression (18). That is, just as the two domains associated with a particle—the group and phase domains—differ by a rotation of $\pi/2$ radians, which corresponds to interchanging real and imaginary components, we will assume here that the second solution can also be obtained from the first by similarly exchanging real and imaginary quantities. Multiple possibilities exist for such a formulation:

$$(\pm i \pm \epsilon)^n \tag{20}$$

Fig. 31 depicts the case $(i+\epsilon)^n$. As observed, this too produces a discrete rotation. However, in this case, the values of the timeline rotate by approximately $\pi/2$ radians with each increment in n. This behavior stems from the approximation $(i + \epsilon) \approx i$ for small ϵ, where the powers of

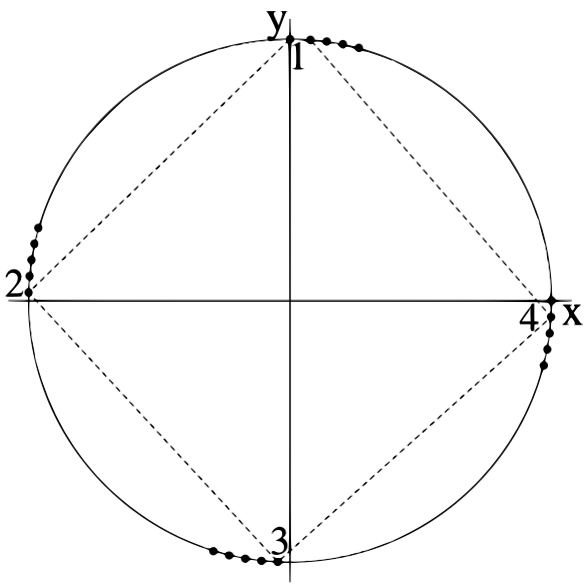

Fig. 31 Graphical representation of $(i+\epsilon)^n$ for a fixed value $\epsilon = 2^{-6} = 0.015625$, and various values $n = 0, 1, 2, 3, \ldots, 20$. The labels $1, 2, 3$, and 4 indicate the positions corresponding to $n = 1, 2, 3, 4$. The dashed lines illustrate values that rotate by approximately $\pi/2$ radians at each step.

i cycle through the values $i, -1, -i, 1, \ldots$, which are each separated by $\pi/2$ radians. The other variants in expression (20) either reverse the direction of rotation or slightly shift the overall figure.

8 A Particle as a Discrete Collective Spacetime Rotation

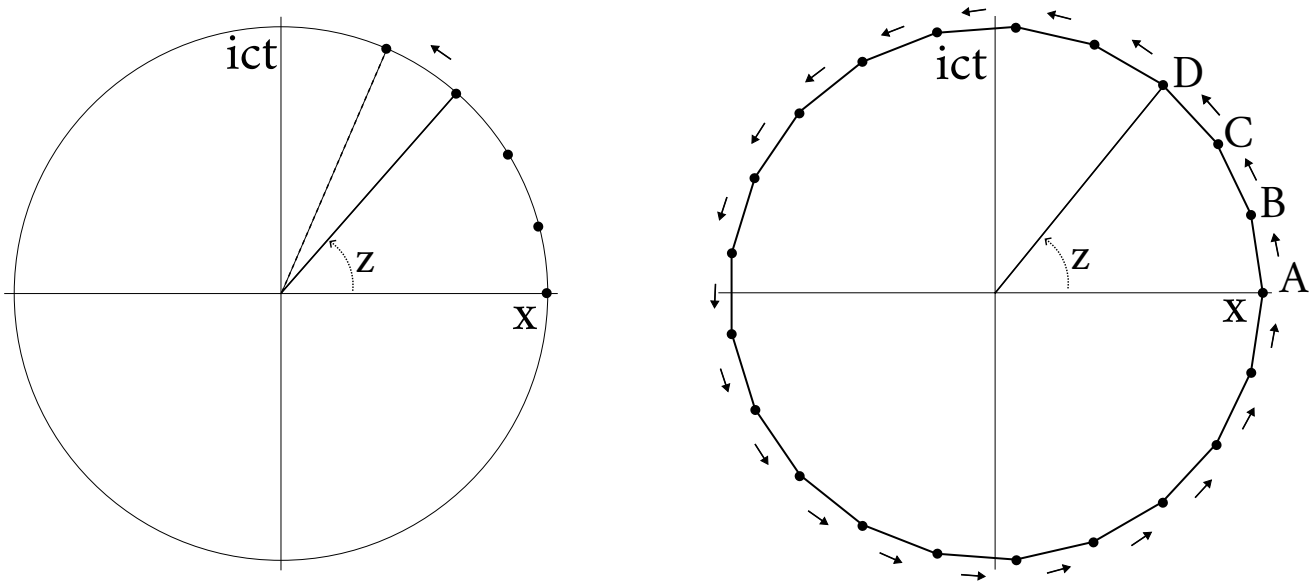

Fig. 32 **Left:** According to the first solution of the timeline—Eq. (18)—, at each beat of proper time a new element is created. However, to unify this picture with the concept of particle as a spacetime rotation, several conceptual shifts must be introduced, such that it ends up becoming a collective performance in which the elements A, B, $C\ldots$ advance their positions at each beat of proper time, as shown on the **right**.

In Ref. [18], it was proposed that a body remains in its inertial state by undergoing a uniform rotation in spacetime. Mathematically, this rotation occurs in the complex plane, where the real axis corresponds to space, the imaginary axis to time, the arc length to an interval of proper time and the angle of rotation is, in general terms, a complex value z.

A similar rotation, now in a discrete form (Fig. 32-*Left*), has emerged from the analysis of a system composed of interacting elements. Note that if both scenarios were unified, one would obtain a discrete spacetime rotation which, on the one hand, would continue to incorporate special relativity and gravity [18], while, on the other hand, the discretization would likely give rise to quantum effects.

To move toward this unification, we must assume that the rotations in the complex plane associated with the two timeline solutions—Eqs. (18) and (20)—are in fact spacetime rotations. This assumption carries several implications:

(i) First, it follows that the axes involved in these two rotations—those depicted in Figs. 29 and 31—must correspond to the spatial and temporal axes.

(ii) Furthermore, the rotation angle must be promoted to a complex value z. In particular, within the domain of special relativity, where $v < c$, this value must be a purely imaginary number of the form $z = i\theta$, where θ is the so-called *rapidity*.[15]

(iii) Moreover, instead of associating a physical object with a single element (as we previously identified ourselves with element A), the object must now be identified with the most recently created element. In this way, at each beat of proper time, the object transitions from one point to the next, thereby reproducing the rotation characteristic of inertial motion. That is, each dot in Fig. 32-*Left* represents a specific instant of proper time for the same physical object.

(iv) However, rather than a single line of points advancing along the perimeter of the circle as in Fig. 32-*Left*, one must adopt the particle representation discussed in Section 4, where a set of elements rotates within the spacetime wheel. [16]

(v) Finally, rather than a continuous rotation, discrete time implies that the elements must change positions at each tick of proper time. That is, elements A, B, C, and so on do not rotate continuously, but shift positions at each temporal increment, as illustrated in Fig. 32-*Right* and, in a more simplified form, in Fig. 33.

This entire sequence of adaptations may appear insufficiently justified at first glance. However, it is important to recall that the underlying goal is to identify a framework capable of unifying both the results of the macroscopic analysis presented in Ref. [18] and those derived here by considering a discrete spacetime.

In summary, following de Broglie, envisioning a particle as a discrete one-dimensional string leads to its representation as a set of points distributed over a wheel of phases. This wheel has been assumed to be equivalent to the spacetime wheel, implying that the oscillation of a single oscillator constitutes a continuous transformation of space into time and vice versa. A particle thus emerges as a set of oscillators engaged in a *collective* rotation in spacetime. However, such spacetime rotations were initially assumed to be continuous, which contradicts the discreteness inherent in the first timeline solution (18). Hence, discreteness must be incorporated into the particle concept. The natural way to achieve this is by positing that, at each beat of proper time, oscillators A, B, C, D, E, etc., exchange positions, as symbolically illustrated in Fig. 33. Accordingly, a particle is represented as a choral performance involving n distinct elements exchanging positions in the spacetime wheel as discrete time advances. This framework will be used to derive the spin.

[15] According to Ref. [18], and following the dynamism introduced by the fundamental cycle, the rapidity is given by $\theta = \omega\tau$, where ω denotes the frequency of spacetime rotation and τ is the proper time, which is now assumed to advance in a discrete manner, i.e., in proportion to the beat of time n.

[16] The transition from a single timeline—advancing discretely in the form of a rotation—to a kind of collective motion involving not just one, but n concurrent timelines, can be interpreted within a framework of interference among possibilities. Previously, we assumed that element A was the first to emerge. However, if we allow any other element to emerge first, then a range of possible configurations may interfere with one another. Since these possibilities might be indistinguishable, they may differ only by a phase. This interference may explain how the timeline can be understood as a *collective performance*.

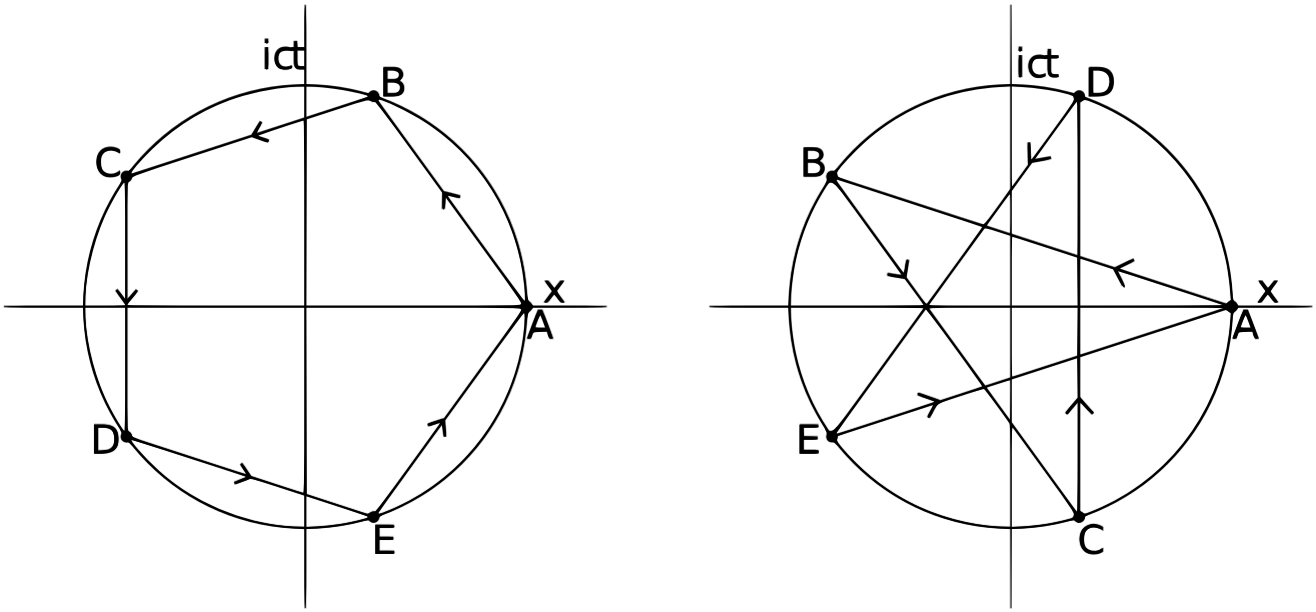

Fig. 33 Left: Representation of a particle in relative motion (see Ref. [18]), now incorporating the notion of discrete time: oscillators A, B, C, D, E exchange phases at each beat of proper time, following the paths indicated by the arrows. **Right:** The same particle represented in a different state of relative velocity.

8.1 Group and Phase Situations

Having interpreted the two timeline solutions (18) and (20) as spacetime rotations, we note that for small ϵ values, the discrete points in the first solution (18) appear to evolve along a straight line (imagine Fig. 32 for $R \gg 1$), suggesting a locally linear evolution. In contrast, the second solution exhibits a clearly *rotational* character, with successive points following the vertices of a square inscribed in the phase wheel.

These two solutions are separated by $\pi/2$ radians, in the sense that one is derived from the other by swapping real and imaginary components. This is reminiscent of the group and phase velocities discussed in Section 2, which also differ by a $\pi/2$ rotation of the axes. It is therefore worth considering whether the two solutions of the timeline correspond to the group and phase regimes:

- The linear nature of solution (18) suggests an association with the group velocity regime, where energy tracks the mass m_o. Therefore, let the first solution be associated with the group regime. In this case, the only energy expression that accounts for both mass and spacetime rotation is $E = m_o c^2$.
- Conversely, the second solution (20) always yields an associated polygon that is a square (see Fig. 31), regardless of the specific polygon or star polygon arising from the first solution. Thus, the energy must be encoded in the square and in the rate at which this square is traversed. This justifies the linear relationship between energy and frequency: $E \propto \omega$, where the proportionality factor must take into account that, in this case, the polygon is a square. Since the proportionality factor is angular momentum L, we conclude that the spin must be deducible from the specific geometric shape of each polygon or star polygon. This analysis will be carried out in Section 9. For now, however, since according to Eq. (13) ω is a phase frequency, the second solution (20) appears to correspond to the phase regime. Hence, this second solution has an associated energy of the form $E = L\omega$.

On the other hand, since the second solution is obtained from the first by exchanging real and imaginary values, this implies a shift in the observer's perspective—from presence to absence. These two solutions therefore describe the same physical situation, perceived from different reference frames (see Fig. 1), and refer to the wave–particle or group–phase duality.

Their equivalence is expressed through the following identity:

$$L\omega = m_o c^2 \tag{21}$$

Proving that the L corresponds to the reduced Planck constant $\hbar$ will be addressed in the next section, where the particle model introduced here will be used to derive spin.

9 Spin Arising from Discrete Spacetime Rotation

In Section 8, it was demonstrated that spacetime rotations occur in a discrete manner, such that the flow of proper time does not progress continuously but instead advances in discrete steps. This discretization was then employed to complete the particle representation introduced in Section 4. Specifically, the implementation of discrete time caused the rotational behavior of the set of elements to shift from being continuous to discrete. As a result, a particle representation akin to those depicted in Fig. 33 was ultimately obtained.

The fact that discretization takes place on a circular topology implies the existence of a limit: the degree of discretization cannot grow indefinitely. Indeed, transitions involving angular separations of π radians between consecutive points on the spacetime circle represent the maximum possible discretization. Moreover, in order to reproduce a stable relativistic configuration between the object and the observer, the discrete steps must form a closed trajectory on the circle. That is, they must define a regular polygon in spacetime, as illustrated in Fig. 34.

At this juncture, it is important to recall the findings of Section 5, where it was shown that those polygons or star polygons which close their trajectories on a 2π-phase circle correspond to minima. Consequently, the associated particles must be unobservable in order to satisfy the uncertainty principle in spacetime. Therefore, to ensure we are describing observable particles, we shall henceforth restrict our discussion to π-radian phase circles.

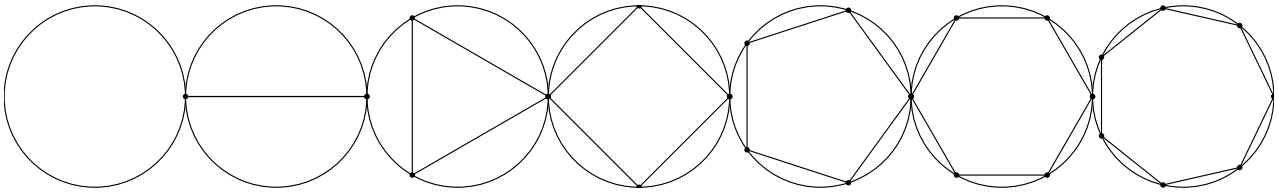

Fig. 34 The figure illustrates, from left to right, the first and most discretized spacetime rotations.

Moreover, regular polygon configurations are not the only stationary shapes permitted by this discretized framework. As shown in Fig. 35, there also exist star polygons, which may rotate either clockwise or counterclockwise.

This raises the question of whether the angular momentum of microscopic particles could be attributed not to rotation in a three-dimensional spatial manifold—as is the case at macroscopic scales—but rather to discrete, stationary rotations in spacetime such as those shown in Fig. 35. As we shall demonstrate, spin indeed emerges from such a spatiotemporal rotation. In particular, this interpretation will enable us to compute the spin associated with the second solution to the timeline equation discussed in Section 7.2, namely, the configuration that traces a square on the spacetime circle. Remarkably, the resulting spin value will be found to be $\hbar$.

This result will allow us to finally recover the expression $\hbar\omega_o = m_o c^2$, thereby completing the derivation of the de Broglie and Planck–Einstein relations that was initiated in Section 3.

9.1 The spin as a discrete spacetime rotation

To investigate the possibility of deriving an expression for spin based on the concept of the particle as a discrete collective performance in spacetime [20–25], let us first recall that, in classical mechanics, the angular momentum of a point mass m_o undergoing uniform circular

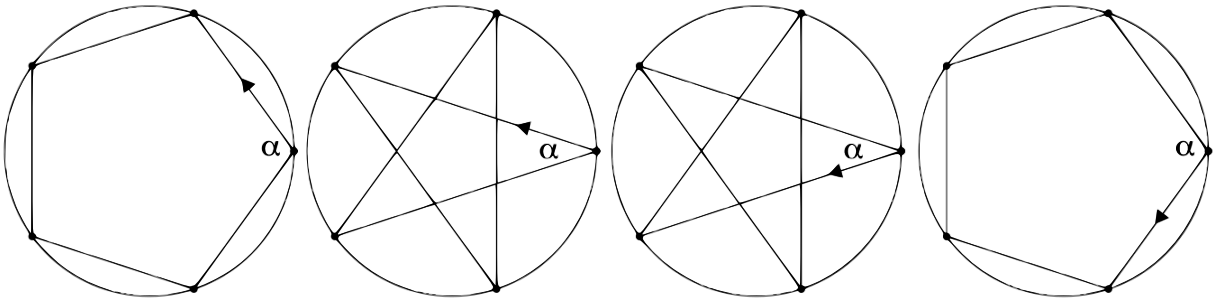

Fig. 35 Polygons or star polygons with $n = 5$ vertices. The angle α represents the *angular visibility* of a given vertex with respect to the two other vertices to which it is connected.

motion with linear velocity v around an axis located at a distance R is, in modulus, given by $L = Rm_o v$.

In our framework, however, it is desirable to define an angular momentum that is independent of mass, radius, or velocity, since it must be applicable to particles such as photons and cannot depend on v, given that all spacetime rotations occur at the invariant speed c. The only remaining possibility is that angular momentum arises solely from the structure of each specific discrete rotation.

With this in mind, we observe from the first two configurations in Fig. 35 that the leftmost figure—corresponding to a *number of points* $n = 5$ and a *step size* $m = 1$—exhibits a greater angular momentum than the adjacent figure to the right (with $n = 5$ and $m = 2$), since its connecting lines extend further from the center of rotation. Intuitively, the closer the lines are to the center, the sharper the arms of the star polygon figure become, indicating a reduction in angular momentum. Therefore, the angle α serves as a proxy for the radial extent of these lines, and hence, as an indicator of the magnitude of the angular momentum.

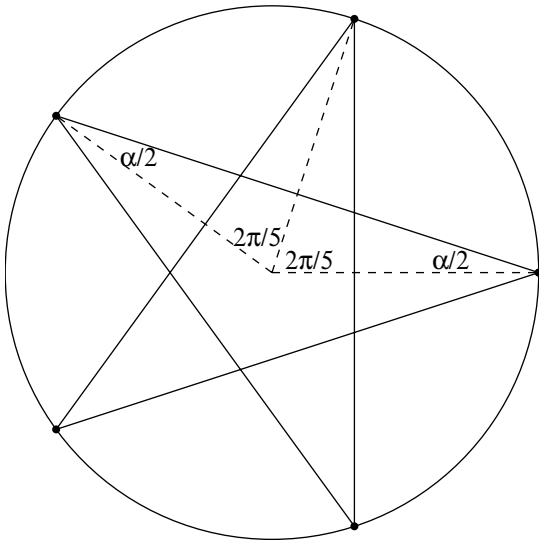

Fig. 36 Depicts a discrete stationary rotation in spacetime with $n = 5$ points and a step size $m = 2$. The sum of the internal angles of the resulting triangle is π: explicitly, $2 \cdot \alpha/2 + 2 \cdot 2\pi/5 = \pi$. In general, the relation $\alpha + m \cdot 2\pi/n = \pi$ holds, which leads to $\alpha = \pi(n - 2m)/n$. The fact that the phase wheel has a total angular extent of π radians does not affect this geometrical derivation.

Since a discrete rotation involves n distinct points that exchange positions at each tick of proper time (as illustrated in Fig. 35), and each such point possesses an *angular vision* quantified by α, it is natural to propose that the angular momentum is proportional to the product $n\alpha$. To express this magnitude in units of full rotations rather than angular measures, we divide by 2π.

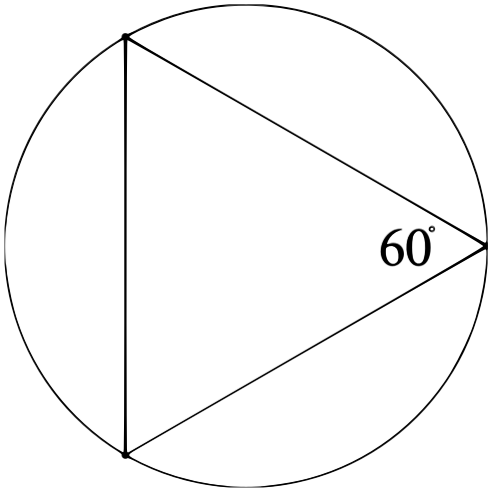

Fig. 37 Discrete rotation with $n = 3$, $m = 1$ and spin=1/2.

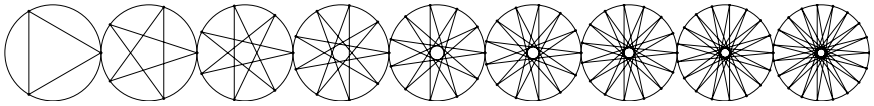

Fig. 38 Examples of discrete stationary rotations in spacetime that yield a spin value of 1/2. These configurations are characterized by an odd number of points n and a step size m such that the arms of the star polygon pass as close as possible to the center of rotation.

Accordingly, we propose the following expression for the angular momentum L associated with a discrete spacetime rotation:

$$L \equiv \frac{n\alpha}{2\pi}\hbar \tag{22}$$

Note, from pure geometry as shown in Fig. 36, that

$$\alpha = \frac{\pi(n-2m)}{n} \tag{23}$$

Therefore, (22) can be written in terms of the number of points n and the value of the step size m as

$$L = \left(\frac{n}{2} - m\right)\hbar \tag{24}$$

where $m = 1, 2, ..., n-1$. Note that this expression corresponds to the quantum values of spin. Indeed, in $\hbar$ units, the possible values of L are

$$L = 0, \pm\frac{1}{2}, \pm1, \pm\frac{3}{2}, \pm2, \pm\frac{5}{2}, \pm3, \pm\frac{7}{2}, ...$$

where negative and positive values account for clockwise and counterclockwise turns (or vice versa).

As an illustrative example, the triangle-shaped discrete rotation shown in Fig. 37 corresponds to a configuration with $n = 3$ and $\alpha = \pi/3$. According to our definition, this yields an angular momentum of $L = \hbar/2$, which could plausibly be associated with the spin of electrons. If the triangular path is traversed in the clockwise direction, it would correspond to a spin of $+1/2$; if traversed counter-clockwise, to a spin of $-1/2$—or vice versa, depending on the chosen convention.

Figures 38 and 39 display representative discrete rotations with spin values of 1/2 and 1, respectively. Figure 40 compiles the initial set of possible discrete spacetime rotations, and Table 2 lists the corresponding spin values derived from them. Furthermore, Fig. 41 highlights the locations of those configurations yielding spin 1/2 values within the full matrix of Fig. 40.

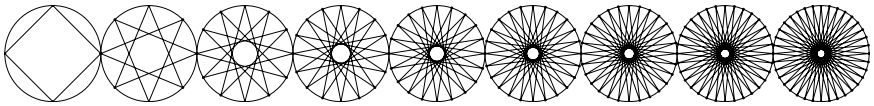

Fig. 39 Examples of discrete stationary rotations in spacetime that yield a spin value of 1. These cases are characterized by even values of n and step size m such that the arms of the star polygon pass near—but do not intersect—the center. Only values of n that are multiples of 4 are considered in this set.

m/n	1	2	3	4	5	6	7	8	9	10	11	12	13
1	0	0	1/2	1	3/2	2	5/2	3	7/2	4	9/2	5	11/2
2	0	0	-1/2	0	1/2	1	3/2	2	5/2	3	7/2	4	9/2
3	0	0	0	-1	-1/2	0	1/2	1	3/2	2	5/2	3	7/2
4	0	0	1/2	0	-3/2	-1	-1/2	0	1/2	1	3/2	2	5/2
5	0	0	-1/2	1	0	-2	-3/2	-1	-1/2	0	1/2	1	3/2
6	0	0	0	0	3/2	0	-5/2	-2	-3/2	-1	-1/2	0	1/2
7	0	0	1/2	-1	1/2	2	0	-3	-5/2	-2	-3/2	-1	-1/2
8	0	0	-1/2	0	-1/2	1	5/2	0	-7/2	-3	-5/2	-2	-3/2
9	0	0	0	1	-3/2	0	3/2	3	0	-4	-7/2	-3	-5/2
10	0	0	1/2	0	0	-1	1/2	2	7/2	0	-9/2	-4	-7/2
11	0	0	-1/2	-1	3/2	-2	-1/2	1	5/2	4	0	-5	-9/2
12	0	0	0	0	1/2	0	-3/2	0	3/2	3	9/2	0	-11/2
13	0	0	1/2	1	-1/2	2	-5/2	-1	1/2	2	7/2	5	0
14	0	0	-1/2	0	-3/2	1	0	-2	-1/2	1	5/2	4	11/2
15	0	0	0	-1	0	0	5/2	-3	-3/2	0	3/2	3	9/2
16	0	0	1/2	0	3/2	-1	3/2	0	-5/2	-1	1/2	2	7/2
17	0	0	-1/2	1	1/2	-2	1/2	3	-7/2	-2	1/2	1	5/2

Table 2 Spin values of those polygons and star polygons in the first 13 columns of Fig. 40.

9.2 The spin as a function of relative velocity

Let us now consider a star polygon like the one shown in Fig. 44. As discussed in Section 8, such a figure represents a particle through a collective motion. In particular, Section 3.1 showed that this many-body phenomenon accounts for the particle's energy E and momentum p. Now we observe that it also explains its spin. Hence, the star polygon representation provides a unified picture encompassing the three fundamental properties of particles: energy, momentum, and spin.

It was also noted that the shape of the star polygon associated with a particle changes with its velocity v_g relative to the observer. In other words, as is well known, both momentum and energy vary with v_g—and so should the spin. Therefore, *it becomes essential to investigate whether the observed spin of a particle evolves through its allowed values as its velocity increases.* If such a test could be performed experimentally, it would offer a powerful means of verifying the validity of this theoretical framework.

9.3 The wave-particle identity

Let us revisit the second solution of the timeline—Eq. (20)—depicted once again in Fig. 42.

As previously argued, this solution is "rotational" in nature and thus related to the phase aspects of matter. Consequently, an energy expression of the form $E = L\omega$ was suggested. According to our spin analysis, the square-shaped configuration corresponds to a unit spin: indeed, the sequence i, i^2, i^3, i^4 contains four points ($n = 4$) and undergoes steps of one unit ($m = 1$). Therefore, by Eq. (24), its angular momentum is $L = \hbar$. As a result, the associated energy becomes $E = \hbar\omega_o$, which is the energy of a photon. This observation implies that the second solution may correspond physically to light.[17] If this second solution manifests as

[17]Interestingly, Feynman and Hibbs [20] attempted to relate the fourth roots of unity—used as statistical weights in their checkerboard path model—to the propagation of particles in spacetime, thereby connecting aspects of spin and chirality to discrete trajectories. However, in their model, this was specifically associated with spin-$\frac{1}{2}$.

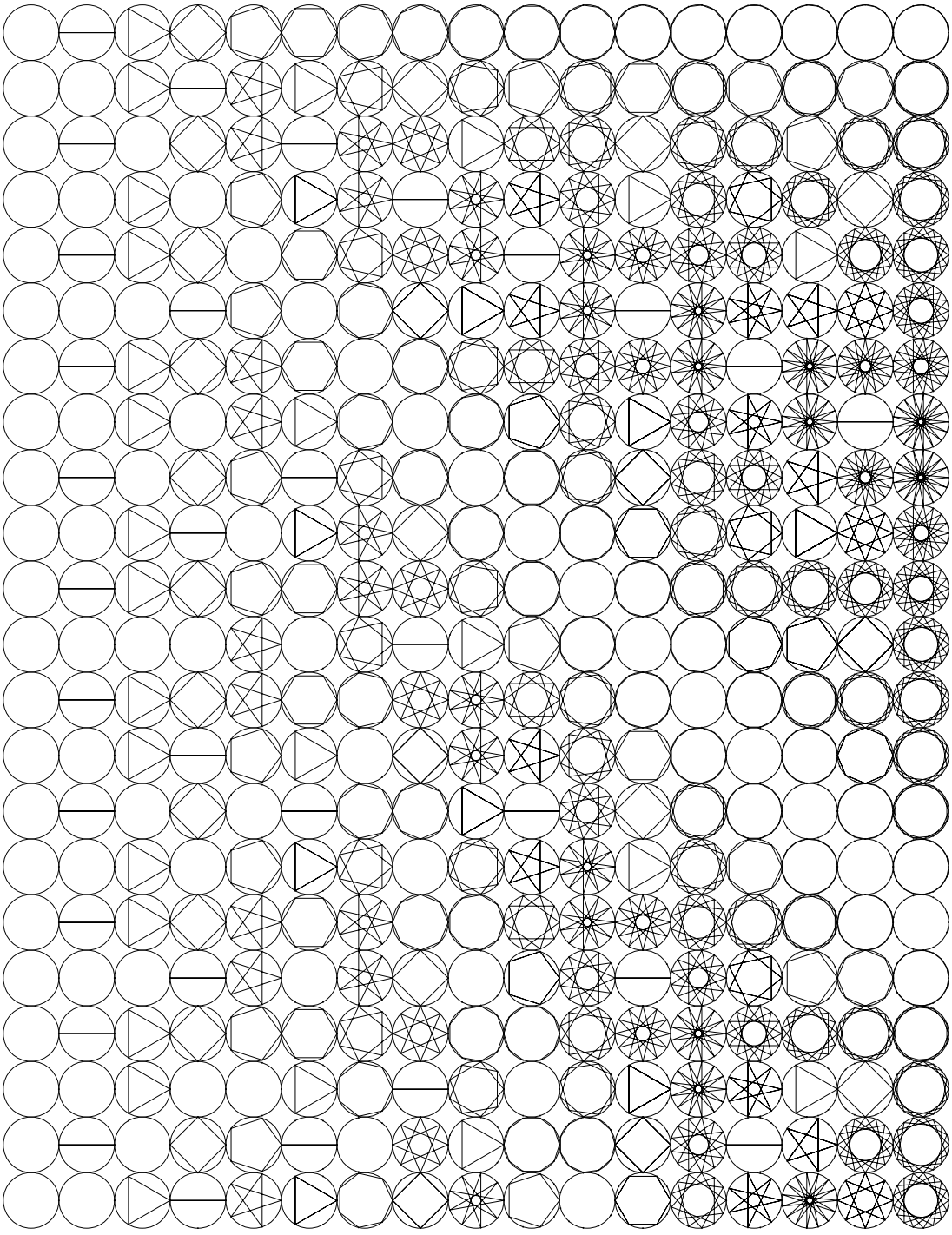

Fig. 40 Table with $i = 1, 2, \ldots, 22$ rows and $j = 1, 2, \ldots, 17$ columns displaying the discrete spacetime rotations (i, j). Each of these configurations can be interpreted as the representation of a specific particle with an associated spin value. The spin values corresponding to the first 13 columns are listed in Table 2.

electromagnetic radiation, then the first solution may be interpreted as matter, as previously suggested.

Thus, based on this analysis, we finally obtain:

$$\hbar\omega_o = m_o c^2 \tag{25}$$

This expression was previously used in Section 3 to derive the de Broglie and Planck–Einstein relations.[18]

[18]The identity (25), which equates a particle's rest energy with an intrinsic frequency, has appeared in various foundational contexts. It was first proposed by de Broglie in the form of a matter wave hypothesis [28], and later echoed in

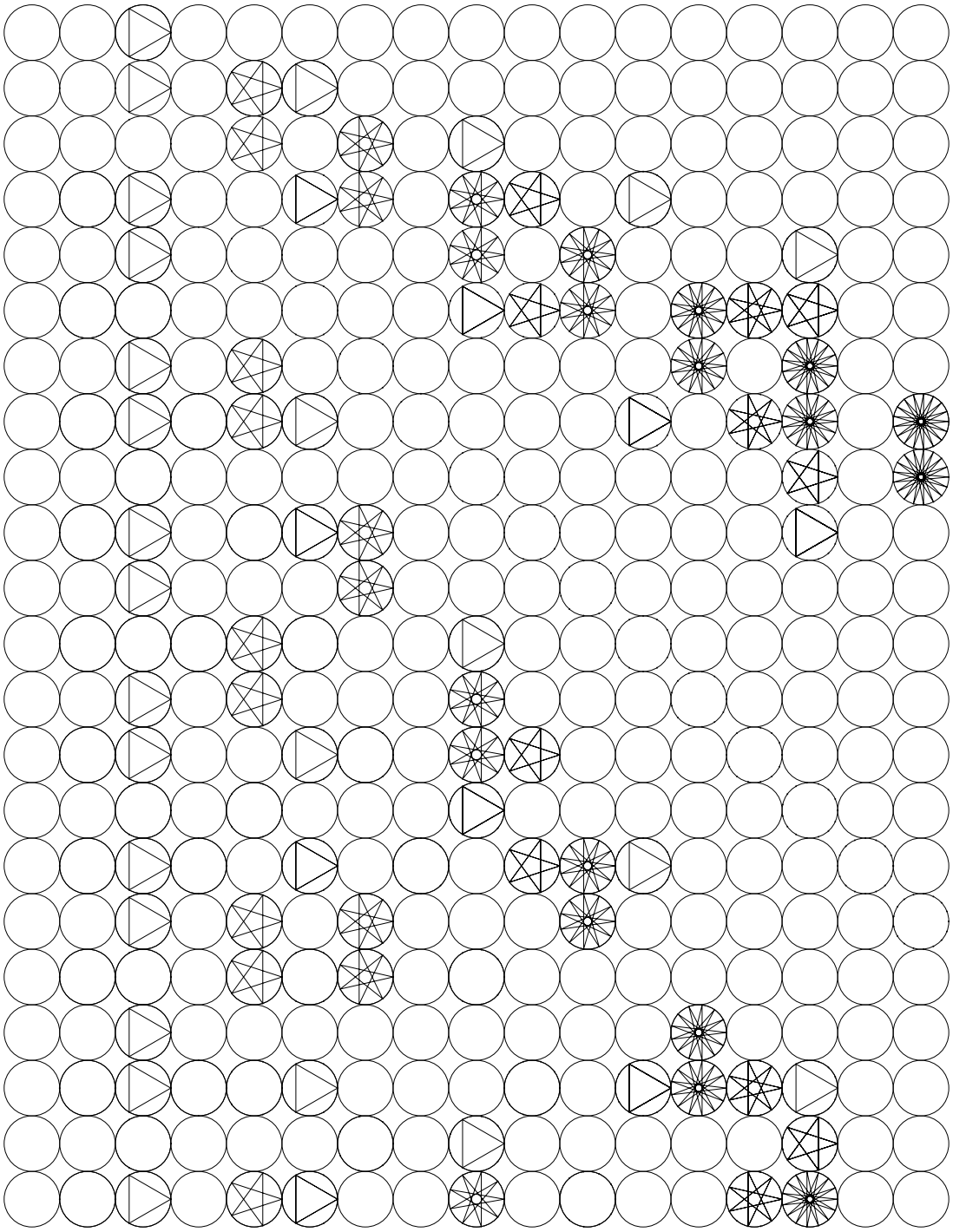

Fig. 41 Locations of those discrete spacetime rotations with spin value equal to $\pm 1/2$ in the table of discrete rotations shown in Fig. 40.

The main conclusion to be drawn is that the angular momentum of microscopic particles might not be related to rotation in physical space, but rather to the very concept of the elementary particle as a collective, discrete, stationary rotation in spacetime. Since this collective motion depends on relative velocity, so too should the spin. Future experimental investigations could be instrumental in testing this hypothesis.

---

the phase evolution of relativistic quantum states [20, 29, 30]. This relation has also been interpreted as describing an internal "clock" associated with the rest mass of the particle [31, 32].

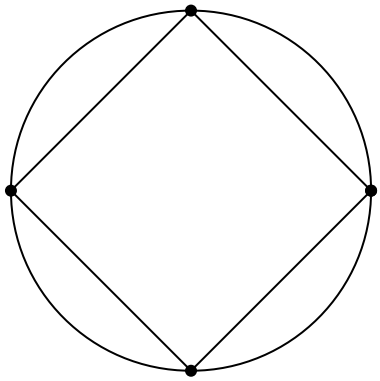

Fig. 42 Discrete spacetime rotation with $n = 4$, $m = 1$, and spin equal to 1.

10 Quantum gravity

Within the framework that conceives elementary particles as discrete collective rotations in spacetime, the current goal is to assign a frequency value to each star polygon as a function of the number of points n and the step size m that define the figure itself. Once this frequency is defined, it will be shown that a length on the plane corresponds to an interval of proper time. This will lead to an alternative expression for the frequency. By equating both expressions and using the relation $hf_o = m_o c^2$ previously derived, an expression for the radius of curvature as a function of n, m, and m_o will be obtained. In other words, each particle will be associated with a specific radius of curvature, whose magnitude will depend on the values of n and m, that is, on the spin. Finally, upon realizing that the relation $g = c^2/R$ holds for star polygons, an expression for quantum gravity will emerge.

10.1 A length on the plane corresponds to an interval of proper time

Newton's first law states that the inertial motion of a body is linear and uniform. We now show that the "inner view"[19] of this law corresponds to the principle of maximum proper time.

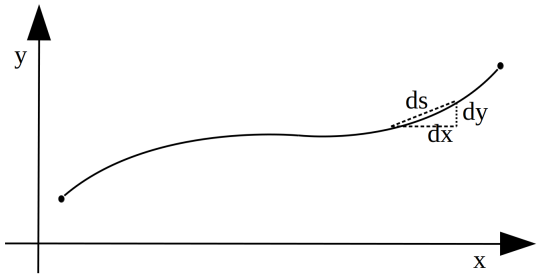

Fig. 43 A path connecting two points on the xy-plane.

Consider two distinct points on the xy-plane and all possible paths connecting them (see Fig. 43). The length s of a given path is computed by:

$$ds^2 = dx^2 + dy^2 \quad \Rightarrow \quad s = \int_{y_1}^{y_2} \sqrt{1 + \left(\frac{dx}{dy}\right)^2}\, dy \tag{26}$$

To interpret this distance s from an "internal" perspective, we follow the argument in Ref. [18] and perform a change of variables by replacing y with ict. Let us proceed in two steps.

[19] The inner view is a concept introduced in Ref. [18] to describe the situation in which the observer is embedded within the physical structure.

First, convert the y-axis into a temporal axis ($y \to ct$):

$$s = c \int_{t_1}^{t_2} \sqrt{1 + \frac{v^2}{c^2}}\, dt \tag{27}$$

Then, adopting the internal viewpoint by introducing the imaginary unit:

$$s = ic \int_{t_1}^{t_2} \sqrt{1 - \frac{v^2}{c^2}}\, dt$$

Using the relation $dt/d\tau = \gamma$ we obtain:[20]

$$ic \int_{t_1}^{t_2} \frac{dt}{\gamma} = ic\, \Delta\tau \tag{28}$$

Thus, the length becomes $ic\Delta\tau$, that is, i times an arc of a circle. Therefore, what is perceived externally as a length in the plane—Eq. (26)—, is internally observed as (ic times) an interval of proper time $\Delta\tau$. This result is fundamental and also permits derivation of the principle of maximum proper time.

Indeed, the principle of maximum proper time asserts that among all possible paths connecting two points, the one corresponding to inertial motion is the one that maximizes $\Delta\tau$. According to Eq. (28), this maximization entails minimizing the integrand $\frac{v^2}{c^2}$. However, if the sign inside the square root is reversed, as in Eq. (27), then minimizing v^2/c^2 corresponds to minimizing the overall integral. Therefore, maximizing proper time from the internal viewpoint is equivalent, from the external viewpoint, to minimizing the spatial length between two given points on the plane—that is, selecting the straight-line path.

Moreover, moving from one point to another in a straight line within a fixed time interval implies constant velocity, which results in a smaller v^2 term compared to a fluctuating velocity about its mean $\langle v \rangle$, since $\langle v \rangle^2 \leq \langle v^2 \rangle$. Hence, from the external perspective, inertial motion corresponds to uniform linear motion on the plane, while internally, it corresponds to the path of greatest proper time.

In conclusion, as previously suggested, the principle of maximum proper time can be interpreted as the relativistic counterpart—or "inner vision"—of Newton's first law of motion [48–50].

10.2 On the relation between mass and radius

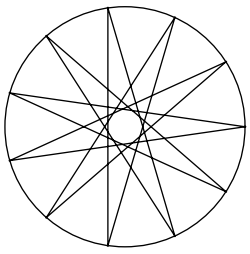

Fig. 44 Representation of a particle with $n = 11$ and $m = 5$.

Let us now define a frequency for each discrete spacetime rotation, i.e., for each spin value. From Fig. 44 it can be seen that the number of discrete turns per unit time performed by a

[20] According to Ref. [18], the expression $\frac{dt}{d\tau} = \gamma$ implicitly incorporates circular geometry.

single element is:

$$f_n^m = \frac{m}{n} f_o \tag{29}$$

where n is the number of elements or arms of the star polygon, m is the step size, and f_o is the frequency associated with each discrete step.[21][22]

The aim now is to derive an expression relating the mass m_o to the values n, m, and R that define a particle.

10.3 The Radius of Curvature of a Star Polygon

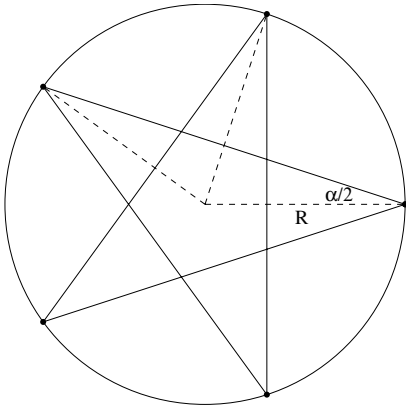

Fig. 45 The length associated with a star polygon is the sum of all its sides. From the figure and in general terms, this is given by $2nR\cos(\alpha/2)$.

If, from classical mechanics, inertial motion corresponds to a straight line, as stated by Newton's first law, and, in relativity, inertial motion corresponds to a trajectory of maximum proper time ($c\Delta\tau$), then, according to the discussion in Section 10.1, the proper period T_n^m associated with a star polygon can be obtained by summing the lengths of all its sides, since a length on the plane corresponds to an interval of proper time. Thus, from Fig. 45, one obtains

$$2nR\cos\frac{\alpha}{2} = cT_n^m$$

Now, by expressing T_n^m as the inverse of the star polygon frequency f_n^m from Eq. (29), we derive an expression for the radius of curvature in spacetime as a function of m_o, n, and m:

$$\left.\begin{aligned} hf_o &= m_o c^2 \\ f_n^m &= \frac{m}{n} f_o \\ 2nR\cos\frac{\alpha}{2} &= cT_n^m \end{aligned}\right\} \implies R = \frac{1}{2m\cos\frac{\alpha}{2}}\frac{h}{m_o c} = \frac{1}{2m\cos\left[\left(\frac{1}{2}-\frac{m}{n}\right)\pi\right]}\frac{h}{m_o c} \tag{30}$$

where Eq. (23) has been used. Note that R appears to be proportional to the *Compton wavelength*, which in SI units is generally much smaller than unity: for instance, for the electron it is of the order of 10^{-13} m, whereas for the Earth it is around 10^{-66} m. Therefore, the proportionality factor $(2m\cos(\alpha/2))^{-1}$ must be examined to determine whether the values of α can make R significant on a macroscopic scale:

- When $\alpha \to \pi$, corresponding to large values of n and small values of m, the radius tends to infinity (flat spacetime). These star polygons resemble a circle.

[21] f_o would be equivalent to the *sampling frequency* in the Discrete Fourier Transform (DFT).

[22] If a physical object is observed to undergo a discrete spacetime rotation from an observer's viewpoint, as illustrated in Fig. 44, it can be said to periodically return to a state of zero relative velocity ($\theta = 0$). As such, it might be interpreted as exhibiting a form of *spacetime vibration*. It would be interesting to investigate whether this bears any correspondence to the Zitterbewegung effect [51, 52].

- When $\alpha \to 0$, which occurs when $m \sim n/2$, the radius becomes $(2m)^{-1}$ times the corresponding Compton wavelength. This leads to low values of R and hence high spacetime curvatures. These are star polygons with sharp arms, as illustrated in Fig. 46.

Since low values of n imply a high level of discretization and thus enhancement of quantum phenomena, which predominantly manifest at microscopic scales, one may interpret microscopic particles as exhibiting large spacetime curvatures. For instance, in the case of the electron, which has spin 1/2 and therefore $n = 3$, the associated radius of curvature remains of the same order as its Compton wavelength. This observation aligns with previous approaches in which the Compton wavelength has been proposed as a natural curvature scale for elementary particles [53–56].

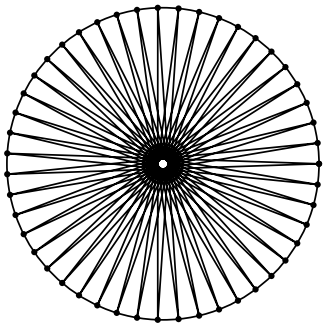

Fig. 46 A star polygon with $n = 47$ and $m = 23$, which clearly deviates from a circular shape. For much larger values of n and $m \sim n/2$, such a figure could represent a black hole.

On the other hand, for massive bodies such as the Earth (mass $\sim 10^{24}$ kg), whose surface gravity (9.8 m/s^2) implies a curvature radius $R \sim 10^{16}$ m via $g = c^2/R$, the factor $(2m\cos(\alpha/2))^{-1}$ would be of the order of 10^{82}. This suggests that α must be extremely close to π, corresponding to nearly flat spacetime.

Therefore, the factor $(2m\cos(\alpha/2))^{-1}$ in Eq. (30) appears to determine, along with the mass, the "*size of the spacetime region*" associated with a particle. Specifically, when n is small—as is expected for microscopic systems—the radius of curvature is also small, effectively confining the particle to a small region of spacetime. In contrast, for massive bodies, where n is assumed large, the value of m determines whether the radius is large (as for the Earth) or small (as for a black hole).

Since the value of m also determines the spin, we may conclude that, for a given particle—i.e., fixed n and f_o—the greater the absolute value of the spin (i.e., the smaller the value of m), the larger the radius R. This relationship is illustrated in Fig. 47.

In black holes, the value of m is expected to be maximal (i.e., $m \sim n/2$) because their volume is extremely small relative to what would be expected given their mass. As a result, the associated spin value should be very low, potentially leading to a very weak magnetic field. Fig. 46, when extended to larger values of n, could serve as an intuitive visualisation of a black hole as a quantum object.

Finally, note that according to the relation $hf_o = m_o c^2$, the mass m_o does not depend on the step size m, thereby allowing different spin values to be associated with the same mass, as expected.

10.4 An Expression for Quantum Gravity

We now aim to show that the centripetal expression for gravity, $g = c^2/R$, remains valid at the microscopic level, particularly in the context of polygons or star polygons. This, together with Eq. (30), will yield a quantum-level expression for g.

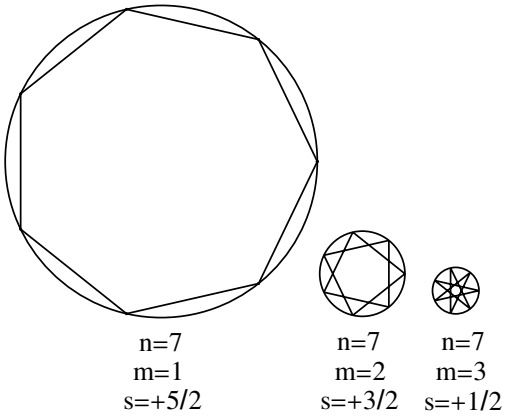

Fig. 47 Illustrates how the radius of curvature associated with a given particle varies for different spin values. In this case, $n = 7$. As the spin decreases from $+5/2$ to $+1/2$, the radius of curvature also decreases according to Eq. (30).

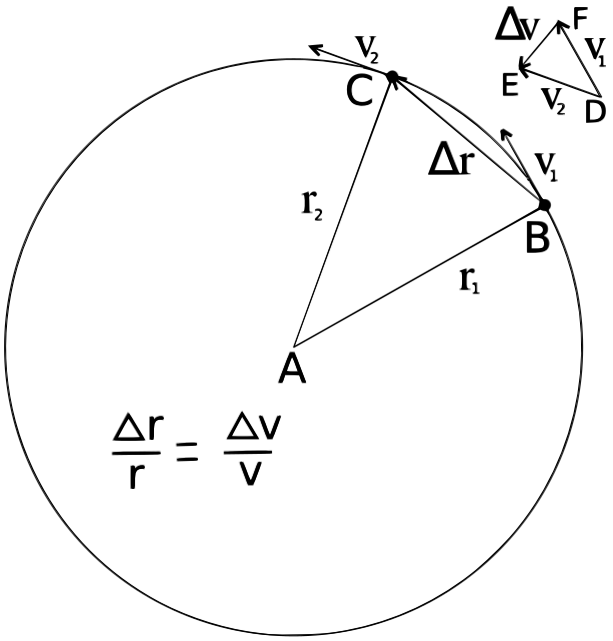

Fig. 48 Illustration of a particle undergoing uniform circular motion (UCM). Triangles ABC and DEF are similar.

From Fig. 48, the similarity of triangles leads to the relation:

$$\Delta v = \frac{v}{r}\Delta r$$

This holds for any value of Δr, i.e., it does not rely on the infinitesimal limit. Dividing both sides by $\Delta\tau$ yields:

$$\frac{\Delta v}{\Delta\tau} = \frac{v}{r}\cdot\frac{\Delta r}{\Delta\tau}$$

Here, the term $\Delta v/\Delta\tau$ represents the centripetal acceleration a_o, while the term $\Delta r/\Delta\tau$ can be interpreted as the velocity c, since the length Δr on the plane corresponds to c times the proper time interval $\Delta\tau$ (as shown in Section 10.1). Furthermore, the velocity v on the right-hand side also equals c. Consequently, we find that the generalization of the centripetal acceleration in the case of star polygons remains:

$$a_o = \frac{c^2}{R}$$

Substituting the expression for R from Eq. (30) yields an explicit expression for quantum gravity:

$$g = \frac{m_o c^3}{h} \cdot 2m \cdot \cos\left[\left(\frac{1}{2} - \frac{m}{n}\right)\pi\right]$$

As a final remark, note that the validity of the gravitational expression $g = c^2/R$ in the case of polygons or star polygons implies that shortcuts through spacetime are possible. That is, one does not necessarily need to traverse the perimeter of a circle to go from one spacetime point to another. Instead, "straight" paths can be traced by the vertices of the polygons or star polygons. Taking such shortcuts could give the impression of faster-than-light travel. In the context of a primordial Universe governed by quantum principles, this may be closely related to the necessity suggested by inflationary cosmological models [33, 34].

As a summary of this last section, it has been shown that the frequency f_o should be interpreted as the rate at which discrete steps occur to realise a discrete spacetime rotation, whereas $f_n^m = (m/n)f_o$ was defined as the frequency of the rotation itself. Moreover, the radius of spacetime curvature associated with a given particle was found to depend on its mass (m_o), the number of discrete points (n), and the step size (m) characterizing its corresponding star polygon.

This formulation implies that microscopic particles (with small n values) may be confined to extremely small spacetime regions, while macroscopic bodies ($n \gg 1$) can occupy either large or small regions depending on their corresponding step size m. For instance, in the case of a black hole—where n is expected to be large and $m \sim n/2$—both the radius of curvature R and the spin are expected to be minimal.

Finally, after establishing that the gravitational expression $g = c^2/R$ also holds for non-circular rotations such as those defined by polygons or star polygons, an explicit quantum expression for gravity was derived as a function of the spin parameters n and m.

11 Summary and Conclusions

The first part of this work corresponds to Ref. [18]. There, we began by arguing that, in order to avoid the idea of a Universe arising from spontaneous generation, it is necessary to postulate the existence of a cycle that alternates between two antithetical natures, which we referred to as *presence* and *absence*. This cycle was represented in terms of uniform circular motion and was called the *fundamental cycle*.

To account for the antagonistic nature of presence and absence, we introduced the imaginary unit $\mathbf{i}$, which also expresses the inconceivability of the beyond when experienced from our real perspective. This perspective was termed the "inner view," as it acknowledges the fact that we belong to the structure being described. Applying this new internal perspective to the circle—understood as the representative of the cycle—led to an expression resembling the invariant interval of relativity. This suggested that space may be understood as the physical manifestation of presence, while time corresponds to absence. Thus, the fundamental cycle between presence and absence became interpreted as a kind of rotation in spacetime.

All these ideas were encapsulated in the following transformation[23] $y \to ict$, which, when systematically applied to the equations of the circle and of uniform circular motion, gave rise to the various relativistic expressions.

In particular, when applied to a coordinate change induced by an axis rotation, this transformation yielded the Lorentz transformation. This allowed inertial reference frames to be represented in terms of two coordinate systems with a relative rotation (along with a time-inversion adjustment). In turn, this representation was used to derive various relativistic effects by applying the functions $\cos i\theta$ and $\sin i\theta$ to perform projections, in the same way that sine and cosine are used in Euclidean geometry.

[23] Or Wick rotation.

In this second part, that is, in the present article, we began by showing that the circular foundation of this model naturally imparts a wave-like character to relativity. This has made it possible to define, within the framework of relativity alone, the group and phase velocities v_g and v_p. While v_g corresponds to the relative velocity between the physical body and the observer, v_p, by contrast, is related to the momentum and energy of the body.

To explore this connection further, and following a proposal originally made by de Broglie, we assumed that a particle can be conceived as a discrete chain of oscillators vibrating at the same frequency and in phase. When this system is observed in motion, a phase shift between the oscillators becomes apparent due to the relativity of simultaneity. This phase shift is characterized by a wavelength λ_p, which has been shown to be the one appearing in the relation $p = h/\lambda_p$. In turn, the frequency f_p associated with the phase wave gives rise to the energy through the Planck-Einstein relation $E = hf_p$.

The fact that intrinsic properties of the particle—such as momentum and energy—are so directly linked to the phase shift between oscillators has suggested representing the particle in terms of a *phase wheel*.

Then, since the phase shift between oscillators results from the conversion of time into space and vice versa, we interpreted this moving phase wheel as a rotation in spacetime and, therefore, as another manifestation of the fundamental cycle. In this way, the particle came to be conceived as a set of n distinct points rotating within the wheel of spacetime, each following its fundamental cycle.

Moreover, when deriving the uncertainty principle from the properties of spacetime, an additional conjecture was required. It was necessary to postulate the existence of maxima and minima associated with a particle's momentum. In the case of minima, this implies the existence of certain momentum values for which the particle becomes unobservable or undetectable. To exclude all such non-observable cases, we refined the concept of a particle by restricting the phase wheel—or spacetime rotation—to a π-radian wheel.

At this point, it was observed that this very structure coincides with that of the cosmological model previously developed in Ref. [18]. In that earlier study, the Universe was conceived as a collection of galaxy clusters rotating within the wheel of spacetime—a wheel in which a complete 2π rotation corresponds to two cosmological cycles.

Thus, we asked whether we might be facing the possibility of universalizing the concept of a particle. However, to do so two major issues remained to be addressed. One was to understand the origin of the fundamental identity $hf_o = m_o c^2$, and the other was to determine whether the quantum properties of matter and radiation stem from a spacetime that is essentially discrete, yet appears continuous at macroscopic scales.

To this end, we shifted to a discrete approach by questioning the true nature of time. In response, we considered a set of interacting elements and enumerated all the distinct possibilities for these elements to be either *present* or *absent* within a given scenario. We then arranged these possibilities into a sequence to construct the timeline and assigned algebraic values to them by associating presence with real numbers and absence with imaginary numbers (or vice versa). Proceeding in this way led to the emergence of uniform circular motion in the complex plane—similar to the previously discussed rotations in spacetime, but now discrete.

Given that the particle has two associated domains—the group and phase domains—that differ by a rotation of $\pi/2$ in the complex plane, we exchanged real with imaginary quantities in that first solution of the timeline in order to find a second one. This second solution also turned out to correspond to a rotation in spacetime, but one that is distinctly discrete and follows the vertices of a square.

The first solution was then associated with the domain of group—or particle—properties, and the second with the domain of phase—or wave—properties. Since the group velocity corresponds to the velocity of the particle with mass m_o, we assigned it an energy of the type $E = m_o c^2$. On the other hand, due to the rotational nature of the second solution, we associated

it with an energy of the rotational form $L\omega_o$. These two energy forms, arising from two distinct perspectives—namely, viewing the same phenomenon from the standpoint of presence or absence—were equated as $m_o c^2 = L\omega_o$. This expression encapsulates the wave-particle duality.

To interpret these two solutions of the timeline in terms of spacetime rotations, concessions were required from both sides. On the one hand, the spacetime rotations had to allow for discretization; on the other hand, the two solutions of the timeline could not be understood as isolated single rotations, but rather as a set of simultaneous rotations—that is, not a single element rotating within the spacetime wheel, but a collection of n elements.

Altogether, this led to an evolution of the particle concept, which came to be understood as a collective performance in which, at each tick of proper time, the n elements constituting the particle exchange their positions along a polygons or star polygons inscribed within a π-radian spacetime wheel.

It was observed that this refined concept of a particle naturally accommodates quantum effects such as spin, implying that each spin should be understood as a particular way of realising a stationary and discrete rotation in spacetime. Specifically, we have seen that the number of vertices n and the step size m of the polygon or star polygon correspond to the quantum numbers of angular momentum. In particular, since the polygon associated with the second (i.e., rotational) solution forms a square (Fig. 42), the corresponding spin value was found to be equal to $\hbar$. Substituting this into the previous expression yielded the wave-particle identity $\hbar\omega_0 = m_0 c^2$, thus complementing the previous derivation of the de Broglie and Planck–Einstein relations.

Although representing a particle in terms of a polygon or a star polygon unifies the properties of momentum, energy, and spin within a single structure, it calls for several remarks:

(i) Conceiving a particle as a discrete one-dimensional string is formally equivalent to a discrete rotation in spacetime—that is, to a discrete spacetime.

(ii) A particle may appear under different polygons or star polygons depending on its velocity relative to the observer.

(iii) Only specific values of the velocity lead to a phase wheel that traces a stationary polygon or star polygon. All other non-stationary configurations should be representable as linear combinations of the stationary modes (e.g., via a discrete Fourier transform).

(iv) There exist polygons or star polygons which correspond to minima and should therefore emerge as non-observable particles. In this context, it would be of experimental interest to verify whether increasing the relative velocity of a particle leads to velocity values at which the particle becomes undetectable.

(v) The fact that the polygons or star polygons vary with the particle's relative velocity implies that the associated spin value also varies. This, too, should be subject to experimental verification.

We further emphasized that the proper frequency f_o of the oscillators composing a particle must be interpreted as the number of discrete steps per second occurring during the process of spacetime rotation, whereas $f_n^m = (m/n)f_o$ represents the effective rotational frequency. Additionally, it was found that the radius associated with the curvature of spacetime for a given particle depends on its mass m_o, the number of discrete points n, and the step size m of its star polygon.

This insight led to the understanding that microscopic particles (i.e., with low n) are confined to small regions of spacetime, while macroscopic bodies ($n \gg 1$) may occupy either large or small regions depending on the step value m. For instance, in the case of a black hole—assumed to have large n—if $m \sim n/2$, then both its radius R and its spin are expected to be very small.

Finally, we derived an expression for gravity in terms of the quantum parameters n and m, by recognizing that the relation $g = c^2/R$ remains valid even for non-circular spacetime rotations, such as those described by polygons or star polygons.

This approach differs significantly from those adopted in contemporary physics, particularly in the context of quantum gravity theories [6, 8–11, 14, 15], with string theory [2–4] and loop quantum gravity [12, 16] being the most developed frameworks. There are, however, two crucial points of overlap: first, the idea that elementary objects extend along one dimension, becoming discrete one-dimensional strings rather than point particles (as in de Broglie's conception of the particle); and second, the notion that spacetime itself appears as discrete. In fact, as we have noted, the analysis suggests that these two features are equivalent. Nonetheless, despite these similarities, the present model is characterized by its mathematical simplicity, in the sense that it does not require multiple spatial dimensions, nor does it introduce from the outset a four-dimensional spacetime structure.

On the other hand, the timeline we have assumed, grounded in binary code, leaves a lingering sense of determinism. In this regard, future work will introduce a non-deterministic concept of the timeline, where the binary code represents merely one possibility among a broader spectrum—albeit not an arbitrary one, but rather the optimal choice, i.e., the one capable of generating a timeline with the minimum number of events. In this way, the problem acquires a stochastic component, which may prove interesting to explore in connection with thermodynamic or informational principles [57, 58].

The emergence of polygons and star polygons as fundamental structures underlying the internal dynamics of elementary particles suggests a deep connection between physics and mathematics. These geometric figures are intimately related to the roots of unity in the complex plane and hence to cyclotomic fields, discrete rotations, and group symmetries. Their appearance in the modeling of quantum spacetime supports the idea that physical reality may not be fundamental, but rather emergent from underlying mathematical structures.

This perspective aligns with views expressed by authors such as Tegmark [59] asserting that our physical world is not merely described by mathematics, but is itself a mathematical structure. In the context of the present model, the emergence of physical quantities such as momentum, energy, and spin from purely geometric constructions reinforces the plausibility of such an ontological stance.

References

[1] Green, M.B., Schwarz, J.H., Witten, E.: Superstring Theory vol. 1–2. Cambridge University Press, Cambridge, UK (1987)

[2] Polchinski, J.: String Theory. Vol. I: An Introduction to the Bosonic String. Cambridge University Press, Cambridge, UK (1998)

[3] Polchinski, J.: String Theory. Vol. II: Superstring Theory and Beyond. Cambridge University Press, Cambridge, UK (1998)

[4] Zwiebach, B.: A First Course in String Theory, 2nd edn. Cambridge University Press, Cambridge, UK (2009)

[5] Regge, T.: General relativity without coordinates. Il Nuovo Cimento **19**(3), 558–571 (1961) https://doi.org/10.1007/BF02733251

[6] Penrose, R.: Twistor algebra. Journal of Mathematical Physics **8**(2), 345–366 (1967) https://doi.org/10.1063/1.1705200

[7] Hawking, S.W., Israel, W.: General Relativity: An Einstein Centenary Survey. Cambridge University Press, Cambridge, UK (1979)

[8] Bombelli, L., Lee, J., Meyer, D., Sorkin, R.D.: Space-time as a causal set. Physical Review

Letters **59**(5), 521–524 (1987) https://doi.org/10.1103/PhysRevLett.59.521

[9] Finkelstein, D., Gibbs, M.: Quantum relativity. International Journal of Theoretical Physics **32**(10), 1801–1813 (1993) https://doi.org/10.1007/BF00673470

[10] Hooft, G.: Quantum gravity as a dissipative deterministic system. Classical and Quantum Gravity **16**(10), 3263–3279 (1999) https://doi.org/10.1088/0264-9381/16/10/318

[11] Connes, A., Douglas, M.R., Schwarz, A.: Noncommutative geometry and matrix theory: Compactification on tori. Journal of High Energy Physics **1998**(02), 003 (1998) https://doi.org/10.1088/1126-6708/1998/02/003

[12] Rovelli, C.: Loop quantum gravity. Living Reviews in Relativity **1**(1), 1–75 (1998) https://doi.org/10.12942/lrr-1998-1

[13] Rovelli, C.: Quantum Gravity. Cambridge University Press, Cambridge, UK (2004)

[14] Hartle, J.B.: Spacetime Quantum Mechanics and the Quantum Mechanics of Spacetime (2014). https://arxiv.org/abs/gr-qc/9304006

[15] Loll, R.: Quantum gravity from causal dynamical triangulations: A review. Classical and Quantum Gravity **37**(1), 013002 (2019) https://doi.org/10.1088/1361-6382/ab57c7

[16] Ashtekar, A., Bianchi, E.: A short review of loop quantum gravity. Reports on Progress in Physics **84**(4), 042001 (2021) https://doi.org/10.1088/1361-6633/abed91

[17] Lloyd, S.: Quantum gravity as a quantum computation. arXiv preprint quant-ph/0501135 (2005)

[18] Aupi, X.: The fundamental cycle: A harmonic reinterpretation of relativity and its cosmological implications. Preprint (2024)

[19] Minkowski, H.: Raum und Zeit. Physikalische Zeitschrift, Garden City, NY (1909). English translation in: Lorentz, H. A., Einstein, A., Minkowski, H., Weyl, H. (1952). *The Principle of Relativity*. Dover Publications.

[20] Feynman, R.P., Hibbs, A.R.: Quantum mechanics and path integrals (1965). See also checkerboard models in 1+1D

[21] Penrose, R.: Angular momentum: an approach to combinatorial space-time. Quantum Theory and Beyond, 151–180 (1971)

[22] Han, M., Huang, Z., Zipfel, A.: Emergence of gravitational dynamics from spin foams. Physical Review D **99**(8), 086016 (2019) https://doi.org/10.1103/PhysRevD.99.086016 https://arxiv.org/abs/1812.02110 [gr-qc]

[23] Oriti, D.: The microscopic dynamics of quantum space as a group field theory. Foundations of Space and Time: Reflections on Quantum Gravity (2013) https://arxiv.org/abs/1302.2849 [gr-qc]

[24] Seiberg, N.: Emergent spacetime. The Quantum Structure of Space and Time (2006) https://arxiv.org/abs/hep-th/0601234 [hep-th]

[25] Beachy, D.: Einstein-cartan field equations from braided spin networks. Unified Framework

Project (2024). Disponible a https://unifiedframework.org/paper

[26] Ryder, L.: Spin in gravitation. Universe **7**(12), 498 (2021) https://doi.org/10.3390/universe7120498

[27] Wilczek, F.: Quantum time crystals. Physical Review Letters **109**(16), 160401 (2012) https://doi.org/10.1103/PhysRevLett.109.160401

[28] Broglie, L.: Recherches sur la théorie des quanta. PhD thesis, University of Paris (1925)

[29] Schrödinger, E.: The proper vibrations of the electron. Annalen der Physik (1933)

[30] Hestenes, D.: The zitterbewegung interpretation of quantum mechanics. Foundations of Physics **20**(10), 1213–1232 (1990) https://doi.org/10.1007/BF01889788

[31] Aharonov, Y., Kaufherr, T.: Quantum frames of reference. Physical Review D **30**(2), 368–385 (1984) https://doi.org/10.1103/PhysRevD.30.368

[32] Hestenes, D.: Electron time, mass, and zitterbewegung. Physics Essays **21**(3), 222–231 (2008)

[33] Guth, A.H.: Inflationary universe: A possible solution to the horizon and flatness problems. Physical Review D **23**(2), 347 (1981)

[34] Linde, A.D.: A new inflationary universe scenario: A possible solution of the horizon, flatness, homogeneity, isotropy and primordial monopole problems. Phys. Lett. B **108**(6), 389–393 (1982) https://doi.org/10.1016/0370-2693(82)91219-9

[35] Ashtekar, A., Singh, P.: Loop quantum cosmology: a status report. Classical and Quantum Gravity **28**(21), 213001 (2011)

[36] Bohm, D.: Quantum Theory. Prentice Hall, New York (1951)

[37] Hestenes, D.: Wherefore the wave function? Foundations of Physics **9**, 363–381 (1979)

[38] Penrose, R.: Angular momentum: an approach to combinatorial space-time. Quantum Theory and Beyond, 151–180 (1971)

[39] Planck, M.: On the law of distribution of energy in the normal spectrum. Annalen der Physik **4**, 553–563 (1901)

[40] Einstein, A.: On a heuristic point of view concerning the production and transformation of light. Annalen der Physik **17**, 132–148 (1905)

[41] Feynman, R.P., Leighton, R.B., Sands, M.: The Feynman Lectures on Physics, Vol. III: Quantum Mechanics, pp. 1–8. Addison-Wesley, Reading, Massachusetts (1965). Chap. 1. See Section 1-2: "The uncertainty principle" for the slit-diffraction derivation

[42] Rovelli, C., Smolin, L.: Spin networks and quantum gravity. Physical Review D **52**(10), 5743–5759 (1995) https://doi.org/10.1103/PhysRevD.52.5743

[43] Hestenes, D.: Spin and uncertainty in the interpretation of quantum mechanics. American Journal of Physics **47**(5), 399–415 (1979) https://doi.org/10.1119/1.11691

[44] Popescu, S., Linden, N., Short, A.J., Winter, A.: Entanglement and the emergence of the arrow of time in nonequilibrium systems. Physical Review E **79**, 061103 (2009) https://doi.org/10.1103/PhysRevE.79.061103

[45] Short, A.J., Myschel, T.: Equilibration in finite time of macroscopic quantum systems. New Journal of Physics **14**, 013063 (2012) https://doi.org/10.1088/1367-2630/14/1/013063

[46] —: The Emergence of Time from Quantum Information Dynamics. Preprint (ResearchGate) (2024)

[47] Oriti, D.: Disappearance and emergence of space and time in quantum gravity. arXiv preprint (2013) https://arxiv.org/abs/1302.2849 [gr-qc]

[48] Arthur, R.T.W.: Time, inertia and the relativity principle. McMaster University Studies in History and Philosophy of Science (1995). Preprint available: "Time, Inertia and the Relativity Principle"

[49] Misner, C.W., Thorne, K.S., Wheeler, J.A.: Gravitation. W. H. Freeman and Company, San Francisco (1973). Chap. 16

[50] McMullin, E.: Newton on absolute time. Journal for the History of Astronomy **9**, 90–99 (1978)

[51] Dirac, P.A.M.: The quantum theory of the electron. Proceedings of the Royal Society A **117**(778), 610–624 (1928) https://doi.org/10.1098/rspa.1928.0023

[52] Schrödinger, E.: Über die kräftefreie bewegung in der relativistischen quantenmechanik. Sitzungsberichte der Preussischen Akademie der Wissenschaften, Physikalisch-Mathematische Klasse, 418–428 (1930)

[53] Haramein, N., Rauscher, E.A.: The schwarzschild proton. In: AIP Conference Proceedings, vol. 1303, pp. 95–100. American Institute of Physics, Melville, NY (2010). https://doi.org/10.1063/1.3571395

[54] Carr, B.J.: The black hole uncertainty principle correspondence. Foundations of Physics (2014)

[55] Saravani, M., Aslanbeigi, S., Kempf, A.: Spacetime curvature in terms of scalar field propagators. ArXiv preprint arXiv:1510.02725 (2015)

[56] Santos, W.C., *et al.*: A duality between curvature and torsion. International Journal of Modern Physics D **27**(10), 1847008 (2018)

[57] Jacobson, T.: Thermodynamics of spacetime: The einstein equation of state. Phys. Rev. Lett. **75**, 1260–1263 (1995) https://doi.org/10.1103/PhysRevLett.75.1260

[58] Verlinde, E.P.: On the origin of gravity and the laws of newton. JHEP **2011**(04), 029 (2011) https://doi.org/10.1007/JHEP04(2011)029

[59] Tegmark, M.: The mathematical universe. Foundations of Physics **38**, 101–150 (2008) https://doi.org/10.1007/s10701-007-9186-9